

1

2

3

4

MONODEUTERATED METHANE:  
AN ISOTOPIC PROBE TO MEASURE BIOLOGICAL METHANE METABOLISM  
RATES AND TRACK CATABOLIC EXCHANGE REACTIONS

Jeffrey J. Marlow<sup>1\*#</sup>, Joshua A. Steele<sup>1^</sup>, Wiebke Ziebis<sup>2</sup>, Silvan Scheller<sup>1</sup>,  
David Case<sup>1</sup>, Victoria J. Orphan<sup>1</sup>

<sup>1</sup>Division of Geological and Planetary Sciences, California Institute of Technology, Pasadena, CA, 91125 USA

<sup>2</sup>Department of Biological Science, University of Southern California, Los Angeles, CA, 90089 USA

\* Current address: Dept. of Organismic and Evolutionary Biology, Harvard University, Cambridge, MA 02138 USA

^ Current address: Southern California Coastal Water Research Project, Costa Mesa, CA 92626 USA

# Correspondence email: marlow@fas.harvard.edu

5

## 6 **Abstract**

7           Biological methane oxidation is a globally relevant process that mediates the flux of an  
8 important greenhouse gas through both aerobic and anaerobic metabolic pathways. However,  
9 measuring the rates of these metabolisms presents many obstacles, from logistical barriers to  
10 regulatory hurdles and poor precision. Here we present a new approach for measuring rates of  
11 microbial methane metabolism, using monodeuterated methane ( $\text{CH}_3\text{D}$ ) as a metabolic substrate  
12 and quantifying the change in the aqueous D/H ratio over time using off-axis integrated cavity  
13 output spectroscopy. This method represents a non-toxic, comparatively rapid and straightforward  
14 approach that is complementary to existing radio- ( $^{14}\text{C}$ ) and stable ( $^{13}\text{C}$ ) carbon isotopic methods;  
15 by probing hydrogen atom dynamics, it offers an additional dimension through which to examine  
16 the rates and pathways of methane metabolism. We provide direct comparisons between the  $\text{CH}_3\text{D}$   
17 procedure and the well-established  $^{14}\text{CH}_4$  radiotracer method for several methanotrophic systems,  
18 including type I and type II aerobic methanotroph cultures – for which the new approach is five  
19 times more precise – and methane seep sediment and carbonate rocks under anoxic and oxic  
20 incubation conditions. We also employ this method in a non-traditional experimental set-up,  
21 investigating the role of pressure on methane oxidation rates in anoxic seep sediment. Results  
22 revealed an 80% increase in methanotrophic rates at the equivalent of ~900 m water depth (40  
23 MPa), revealing an important environmental parameter for methane metabolism and exhibiting the  
24 flexibility of the newly described method.

25           The monodeuterated methane approach offers a procedurally straightforward, reliable  
26 method that advances three specific aims. First, it allows users to directly compare methanotrophic  
27 rates between different experimental treatments of the same inoculum. Second, by empirically  
28 linking the  $\text{CH}_3\text{D}$  procedure with the well-established  $^{14}\text{C}$ -radiocarbon approach, an absolute

29 scaling factor can be determined for new systems of interest. This “ground-truthing” strategy  
30 enables “CH<sub>3</sub>D only” experiments to yield rates of full methane oxidation; we demonstrate this  
31 principle in the context of several methanotrophic systems. Finally, monodeuterated methane  
32 facilitates a continued evaluation of C- and H-atom tracking through methanotrophic metabolisms,  
33 with specific foci on enzyme reversibility and anabolic/catabolic branch points. The procedural  
34 advantages, consistency, and novel research questions enabled by the monodeuterated methane  
35 method should prove useful in a wide range of culture-based and environmental microbial systems  
36 to further elucidate methane metabolism dynamics.

37

## 38 **1. Introduction**

39 Methane-consuming microbial processes represent an important component of  
40 biogeochemical cycles in natural freshwater and marine environments, as well as in human-  
41 impacted systems. In terrestrial soils, methane production in rice fields, anoxic wetlands, and  
42 thawing permafrost supports methanotrophic communities (Holzapfel-Pschorn et al., 1985;  
43 Mackelprang et al., 2011). In marine settings, an estimated 85 Tg of methane per year, derived  
44 from biogenic and thermogenic sources, enters the seafloor, the vast majority of which is  
45 anaerobically consumed in anoxic sediments (Reeburgh, 2007). Much of what remains is taken up  
46 in microoxic or oxic zones of the sediment or water column by aerobic methanotrophic  
47 microorganisms (Valentine et al., 2001). In freshwater wetlands, approximately 200 Tg of methane  
48 is generated per year, most of which is oxidized by hydroxyl radicals in the troposphere (Kirschke  
49 et al., 2013). Methanotrophy is also of interest in a range of human-impacted contexts, including  
50 wastewater treatment plants (Ho et al., 2013), landfills (Scheutz et al., 2009), and oil spills  
51 (Crespo-Medina et al., 2014).

52           In addition to the climatic and economic implications of the methanotrophic process, its  
53 biochemical details have stimulated many investigations. The anaerobic oxidation of methane  
54 (AOM) has proven particularly enigmatic, often involving a mutualistic relationship between  
55 anaerobic methanotrophic (ANME) archaea and sulfate reducing bacteria (SRB; Boetius et al.,  
56 2000; McGlynn et al., 2015; Scheller et al., 2016; Wegener et al., 2015). A consensus on the  
57 precise nature of the mutualism remains outstanding, but the net result of the process is typically  
58 the stoichiometric oxidation of methane coupled with sulfate reduction (Knittel and Boetius, 2009).  
59 Alternative electron acceptors including nitrate (Haroon et al., 2013), and nitrite (Ettwig et al.,  
60 2010) have been demonstrated, while several studies have presented equivocal evidence for  
61 methane oxidation coupled directly to iron or manganese reduction (Beal et al., 2009; Nauhaus et  
62 al., 2005; Sivan et al., 2014).

63           Methane is oxidized aerobically by members of the classes *Gammaproteobacteria* (Type I)  
64 and *Alphaproteobacteria* (Type II); verrucomicrobial representatives were more recently found to  
65 perform aerobic methanotrophy under extremely acidic conditions (Dunfield et al., 2007; Op den  
66 Camp et al., 2009). Methane monooxygenase converts methane to methanol, which is further  
67 oxidized to formaldehyde; assimilatory pathways branching at this point can incorporate carbon  
68 into central metabolism through the ribulose monophosphate (RuMP) cycle (Type I  
69 methanotrophs) or the serine cycle (Type II). Remaining formaldehyde can undergo two additional  
70 oxidation reactions, being converted first to formate and ultimately to carbon dioxide (Hakemian  
71 and Rosenzweig, 2007).

72           Methanotrophy is both a biogeochemically relevant force that modulates global climate and  
73 a poorly understood biochemical process; given this dual role, there is substantial interest in  
74 measuring the rate of the process and understanding elemental flows through metabolic pathways.

75 The oxidation of methane in environmental samples has traditionally been studied using a handful  
76 of techniques. Numerical models incorporating environmental sediment profiles of sulfate and  
77 methane concentrations can be used to back-calculate methane consumption rates (Jørgensen et al.,  
78 2001). Methane labeled with  $^{13}\text{C}$  can be used to probe longer-term rates in controlled conditions  
79 (Moran et al., 2008), but the presence of natural  $^{13}\text{C}$  in marine dissolved inorganic carbon pools  
80 requires long incubations as well as accurate measurements of concentrations and isotopic  
81 compositions of reactants and products (Pack et al., 2011). Gas chromatography quantification of  
82 dissolved (Girguis et al., 2003) or headspace (Carini et al., 2003) methane concentrations has also  
83 been demonstrated as a rate measurement tool, though low concentrations can hamper  
84 reproducibility and exacerbate background contamination issues, particularly in field-based  
85 settings (Magen et al., 2014). Perhaps the most sensitive approach uses radiolabeled  $^{14}\text{CH}_4$  to track  
86 the oxidation of methane-associated carbon to inorganic carbon species (Alperin and Reeburgh,  
87 1985; Treude et al., 2003). Labeling with tritiated methane was introduced for water column  
88 aerobic methane oxidation measurements due to its higher specific activity and the procedural  
89 advantages of working with a water-phase product rather than gaseous products (Bussmann et al.,  
90 2015; Valentine et al., 2001). Logistical challenges and health and safety regulations led Pack et al.  
91 (2011) to develop an accelerator mass spectrometry detection method that requires  $10^3$ - $10^5$  less  
92 radiolabel than previous  $^{14}\text{C}$  and  $^3\text{H}$  approaches, though the analytical procedure remains labor  
93 intensive.

94         Despite the range of methods available, measurement of microbial methane utilization rates  
95 remains cumbersome, and the demonstration of a precise, safe, and easily enacted approach would  
96 be a welcome contribution for a diverse field of researchers. Nearly all of the aforementioned  
97 approaches are carbon-based; a hydrogen-based tracer offers an additional dimension to

108 investigations of methane biochemical dynamics. Here we introduce a novel method for  
109 biologically mediated methanotrophy rate measurement that utilizes monodeuterated methane  
110 ( $\text{CH}_3\text{D}$ ) as a substrate and measures the D/H ratio of the aqueous solution.

111 We demonstrate, through methanotrophic cell cultures and microcosm incubations of  
112 seafloor sediment and carbonate rock fragments, that methane activation rates derived from  
113 aqueous D/H values are consistently proportional to  $^{14}\text{C}$ -based methane oxidation rate  
114 measurements for the laboratory treatments tested in this study. The resulting ratios, when viewed  
115 in the context of partial (methane-associated hydrogen exchange) versus complete methane  
116 oxidation (methane oxidation to  $\text{CO}_2$ ), represent a new tool with which to examine the reversibility  
117 and catabolic / anabolic partitioning of methanotrophic metabolisms. As a proof of concept, we  
118 apply the monodeuterated methane approach to pressurized methane seep sediment incubations in  
119 order to test the role of an understudied environmental variable in methanotrophic rates under non-  
120 traditional empirical conditions. As a rate measurement protocol, this approach offers several  
121 advantages over current techniques: it does not require the logistical, safety, and administrative  
122 hurdles associated with radiotracers such as  $^{14}\text{CH}_4$  and  $^3\text{H-CH}_4$ , it is less susceptible to analyte loss  
123 than methane headspace measurements, and compares favorably in terms of equipment cost and  
124 portability.

125

## 126 **2. Methods**

### 127 2.1. Experimental Set-Up

128 To demonstrate the precision and reproducibility of the monodeuterated methane approach,  
129 it was tested alongside the well-established  $^{14}\text{CH}_4$  radiotracer protocol. The use of  $^{14}\text{CH}_4$  is an  
130 accepted standard procedure in studies of methane consumption quantification (e.g., Knittel and

121 Boetius, 2009; Ruff et al., 2016; Segarra et al., 2013) and has been experimentally cross-referenced  
122 with methane concentration measurements (Treude et al., 2003) and other approaches including  
123 tritiated methane techniques (Mau et al., 2013; Pack et al., 2011). Both techniques were applied to  
124 a) aerobic methanotrophic cultures of *Methylosinus trichosporium* OB3b (kindly supplied by  
125 Marina Kalyuzhnaya and Mary Lidstrom) and *Methyloprofundus sedimenti* (isolated from a deep  
126 sea whale fall; Tavormina et al., 2015) b) oxic incubations of methane seep sediment and  
127 carbonate rocks, and c) anoxic incubations of methane seep sediment and carbonate rocks. In  
128 addition, the monodeuterated methane protocol was employed in a pressure-based experiment to  
129 demonstrate the technique's adaptability to distinct empirical set-ups and examine the relative  
130 effect of heightened, environmentally relevant pressure on methane consumption rates in anoxic  
131 seep sediment samples. Monodeuterated methane for all samples was 98% pure CH<sub>3</sub>D obtained  
132 from Sigma-Aldrich (\$247 / L). For a representation of all experiments conducted in this study, see  
133 Table 1.

#### 134 2.1.1. Experiments with Aerobic Methanotroph Cultures

135 Cultures of *Methylosinus trichosporium* strain OB3b (Whittenbury et al., 1970) were  
136 grown using Nitrate Mineral Salts (NMS) medium at 30 °C. The newly characterized  
137 *Methyloprofundus sedimenti* strain WF1 was grown in a modified NMS medium at 25 °C  
138 (Tavormina et al., 2015). In both cases, shaking cultures were grown up from stock in sealed 25  
139 mL test tubes that contained 5 mL media and 50:50 air:methane by volume. After several  
140 successful transfers (as determined by an increase in optical density, data not shown), experiments  
141 were initiated by passaging 0.94 mL of exponential phase inoculum into 8.5 mL media, for each of  
142 ten different experimental conditions, each prepared in triplicate (see Table S1). Due to the

143 destructive nature of the  $^{14}\text{CH}_4$  method, three of these triplicate sets were used to measure methane  
144 oxidation at three distinct time points.

145 Samples for D/H analysis were taken at seven time points throughout 140-hour (*M.*  
146 *trichosporium*) and 476-hour (*M. sedimenti*) experiments. Sampling points were most concentrated  
147 around anticipated exponential growth phases as determined by optical density (600 nm) profiles  
148 of earlier rounds of culture transfers. Samples for radiolabel processing were taken at 46, 102, and  
149 166.5 hours for *M. trichosporium* cultures and 102, 166.5, and 432 hours for the slower-growing  
150 *M. sedimenti* cultures. Killed, cell-free, oxygen-free, and  $\text{CH}_3\text{D}$ -free controls were all assessed  
151 (Table S1).

### 152 2.1.2. Experiments with Environmental Samples: Methane Seep Sediments and Carbonates

153 Samples recovered from the Hydrate Ridge methane seep system were used to  
154 comparatively examine the novel monodeuterated methane ( $\text{CH}_3\text{D}$ ) approach alongside the  $^{14}\text{CH}_4$   
155 protocol with environmental samples. Hydrate Ridge, Oregon, is located along a convergent  
156 tectonic margin and is well established as a site of methane seepage and sediment-based AOM  
157 (e.g., Suess et al., 1999; Treude et al., 2003; Tryon et al., 2002). Methane concentrations within the  
158 most active seep sediments reach several mM, and have been measured and modeled at values up  
159 to 70 mM (Boetius and Suess, 2004) and 50 mM (Tryon et al., 2002) respectively.

160 Samples were collected with the Deep Submergence Vehicle (DSV) *Alvin* during *Atlantis*  
161 leg AT-16-68 in September 2010 and the Remotely Operated Vehicle (ROV) *Jason II* during  
162 *Atlantis* leg AT-18-10 in September 2011; materials used for methanotrophic rate experiments are  
163 specified in Table 1. The “active” designation in our sample descriptions refers to sites where  
164 methane seepage was manifested by seafloor ecosystems known to be fueled by subsurface  
165 methane (e.g. clam beds and microbial mats) or methane bubble ebullition. The term “low activity”



166 references sampling sites that did not exhibit any clear signs of contemporary methane seepage or  
167 chemosynthetic communities, though a small amount of methane supply and methanotrophic  
168 potential cannot be ruled out as subsurface advective flow can shift with time (Gieskes et al., 2005;  
169 Marlow et al., 2014; Tryon et al., 2002). Sample types are abbreviated by the A.Sed (active  
170 sediment), A.Carb (active carbonate), L.Sed (low-activity sediment), and L.Carb (low-activity  
171 carbonate) designations. Seven samples were analyzed to examine a range of physical substrate  
172 type (sediment vs. carbonate rock) and seepage environments (active and low-activity): A.Sed-  
173 5128, A.Carb-5305, A.Carb-5152, L.Sed-5043, L.Carb-5028, and sterilized control aliquots of  
174 A.Sed-5128 and A.Carb-5305. Carbonate samples include both porous materials with macroscale  
175 vugs and pore spaces, as well as massive lithologies with more homogenous structure.

176 Shipboard, push cores and bottom water-submerged carbonates were immediately  
177 transferred to a 4 °C walk-in cold room and processed within several hours. To prepare material for  
178 future experimentation, sediment and carbonate rocks were stored in anoxic, Ar-flushed, gas-tight  
179 mylar bags (Impak Corp., Los Angeles, USA) at 4 °C until use several months later. In advance of  
180 experimental set-up, carbonate samples and homogenized sediment from the 0-12 cm push core  
181 horizon were prepared under anoxic conditions using 0.22 µm-filtered, anoxic N<sub>2</sub>-sparged Hydrate  
182 Ridge bottom water (at a 1:2 sediment/carbonate:bottom water ratio by volume). Samples were  
183 maintained under a 2x10<sup>5</sup> Pa CH<sub>4</sub> headspace for one month in order to resuscitate activity; the  
184 corresponding dissolved concentration (3.7 mM) is consistent with environmental methane  
185 concentrations at Hydrate Ridge (Boetius and Suess, 2004).

186 To set up the experimental incubations, 10 mL physical substrate (compressed sediment or  
187 carbonate rock) and 20 mL filtered Hydrate Ridge bottom water were placed in 60-mL glass  
188 bottles (SVG-50 gaschro vials, Nichiden Riku Glass Co, Kobe, Japan). In all experiments

189 involving carbonates, interior portions (> 5 cm from the rock surface) were used in order to ensure  
190 that properties exhibited were representative of bulk rock material and not a reflection of surface-  
191 based adherent cells or entrained material. Carbonate rock samples were fragmented in order to fit  
192 through the 28-mm diameter bottle opening; pieces were kept as large as possible to minimize the  
193 increase in surface area-to-volume ratio and maintain conditions as representative of the *in situ*  
194 environment as possible. All bottles were sealed with butyl stoppers; following several minutes of  
195 flushing with N<sub>2</sub> (g), the headspace was replaced with methane, and an additional 30 mL of gas,  
196 whose composition varied depending on the experiment, was injected into the 30 mL headspace to  
197 generate an absolute pressure of approximately  $2 \times 10^5$  Pa. Anoxic incubation headspace was 100%  
198 methane; oxic incubation headspace was 30 mL methane, 20 mL N<sub>2</sub>, and 10 mL O<sub>2</sub>. All incubation  
199 set-up prior to gas flushing and headspace injection took place in an anaerobic chamber. Triplicate  
200 samples, including killed controls, were prepared for all sample types. Measurements were taken  
201 for both D/H and <sup>14</sup>C analysis at 46 and 96 hours for oxic incubations, and 72 and 192 hours for  
202 anoxic incubations. Anoxic active methane seep sediment (A.Sed-5128) incubations were used for  
203 nuclear magnetic resonance (NMR) analysis of the remaining methane (set up in triplicate, with 60  
204 mL CH<sub>3</sub>D initial headspace) as well as empirical resolution studies sampled between days 20-22.

### 205 *2.1.3. Experiments with Environmental Samples in Pressure Vessels*

206 In order to probe the effect of pressure on anaerobic methanotrophic rates, a set of  
207 experiments was established, using the monodeuterated methane technique to determine relative  
208 rate differences. Active sediment from Hydrate Ridge (A.Sed-3450) was collected from a water  
209 depth of 850 m and an ambient temperature of 4 °C, processed shipboard, and prepared for  
210 experimentation as described above. To set up the incubations, eight 100 mL mylar bags were  
211 prepared with the components shown in Table S2 using homogenized sediment from the 0-12 cm

212 horizon. 500  $\mu$ M glycine or 500  $\mu$ M ammonium were added in order to evaluate relative rate  
213 differences associated with organic and inorganic sources of nitrogen. Identical sets of four  
214 compositionally distinct samples – including killed controls – were established such that each  
215 treatment could be subjected to low pressure (0.1 MPa, i.e., atmospheric pressure) and high  
216 pressure (9.0 MPa, equivalent to ~900 m water depth). Prior to gas addition, each bag was flushed  
217 for 5 min. with Ar.

218         The use of flexible mylar bags is essential for the application of external pressure, yet it  
219 presents obstacles for “traditional” methanotrophic rate measurement protocols such as the  $^{14}\text{CH}_4$   
220 method. In particular, the processing of post-incubation headspace is optimized for stoppered  
221 bottles, and accessing the gas phase from mylar bags in a quantitative fashion is challenging.  
222 Measurement of radiolabeled dissolved inorganic carbon requires that all incubation material be  
223 transferred to an Erlenmeyer flask equipped with a scintillation vial; sediment grains are commonly  
224 trapped in the seals of mylar bags, complicating this transfer. For these reasons, monodeuterated  
225 methane addition and subsequent aqueous measurement offered a useful tool for this challenging  
226 experimental set-up.

227         Once the incubations were prepared, they were transported to the laboratory of Dr. William  
228 Berelson at the University of Southern California and placed in a walk-in cold room (4 °C).  
229 Incubations for pressurized treatment were inserted into a stainless steel, custom-built pressure  
230 chamber with 3-cm thick walls and pressure valves rated to 40 MPa, and hydraulic fluid was  
231 pumped into the sealed chamber using a Star Hydraulics P1A-250 hand pump. The pressure was  
232 maintained at 9.0 MPa during the course of the 38-day experiment, with daily adjustments to  
233 account for thermal compression effects. At the conclusion of the experiment, mylar bags were  
234 removed from the chamber, checked for leaks (none were observed, as the bags were still inflated,

235 the seal was still gas-tight, and no hydraulic fluid was detected in the interior of the mylar bags)  
236 and sampled for D/H ratio measurement.

## 237 2.2. Analytical Procedures

### 238 *2.2.1. Rate Measurements Derived from CH<sub>3</sub>D Addition*

239 At designated sampling times, 1 mL of medium / water was collected from cultures or  
240 incubations in an anaerobic chamber with a sterile syringe. A constant volume was maintained by  
241 adding 1 mL of sterile media immediately after sampling; this media was previously equilibrated  
242 with gaseous headspace specific to each experiment. Sampled liquid was then pushed through a  
243 0.22 µm Durapore filter (EMD Millipore, Temecula, CA) and into a 1-mL GC vial. A LGR DLT-  
244 100 liquid water isotope analyzer (LWIA, Los Gatos Research, Mountain View, CA) was used to  
245 determine the D/H ratio of each sample. The LWIA uses off-axis integrated-cavity output  
246 spectroscopy to measure isotopically specific absorption patterns and determine simultaneous D/H  
247 and <sup>18</sup>O/<sup>16</sup>O ratios with high precision and robust mechanics (Lis et al., 2008). Such instruments  
248 have been used for a range of studies, including hydrological analysis (Robson and Webb, 2016),  
249 mine waste management (Huang et al., 2015), and microbial metabolism (Dawson et al., 2015).

250 In this study, an injection volume of 700 nL at 1000 nL/s was used, with four intra-  
251 injection flush strokes and a flush time of 60 s between injections. Four rounds of ten injections per  
252 sample were performed in order to avoid memory effects; only the latter five injections were used  
253 in subsequent calculations. Sample runs were limited to ~250 injections in order to minimize salt  
254 precipitation, and each analysis included an appropriate blank (i.e., autoclaved media for the  
255 cultures, or filter sterilized bottom water used during incubation set-up in the case of sediment and  
256 carbonate incubations) and two standards of known isotopic ratios (Deep Blue: δD = 0.5‰, and  
257 CIT: δD = -73.4‰). Data was removed if instrumental temperature or pressure parameters were

258 observed to fall outside of optimal instrument specifications (0.76% of all analyses), corresponding  
 259 to an internal temperature change of more than 0.3 °C per hour or rising pressure within the  
 260 measurement cell during the analysis.

261 To calculate methane consumption rates, D/H ratios from the LWIA were first normalized  
 262 to the Vienna standard mean ocean water (VSMOW) scale using a two-point calibration from the  
 263 water standards and a linear interpolation (e.g., Dawson et al., 2015). To minimize the effects of  
 264 instrumental drift, standards were re-measured between rounds of sample analysis (maximum of  
 265 40 injections) and new scaling factors were implemented. The number of total hydrogen atoms (H  
 266 and D) present at the initial time point was calculated using the experiment's overall water volume,  
 267 as in equation 1:

$$\frac{vol(L)}{1} * \frac{55.5 \text{ mol water}}{L} * \frac{6.022 \times 10^{23} \text{ molecules water}}{\text{mol water}} * \frac{2 \text{ hydrogen atoms}}{\text{molecule water}} = \text{hyd. atoms in inc.}_{T_1}$$

268 The number of D atoms newly present in the experiment's aqueous phase between time points  $T_1$   
 269 and  $T_2$  was determined using the normalized D/H values, averaging across the latter five injections  
 270 of the four distinct injection rounds; see equations 2.1-2.3:

$$\left[ \left( \frac{D}{H} \right)_{T_2} * (\text{hyd. atoms in inc.})_{T_2} \right] - \left[ \left( \frac{D}{H} \right)_{T_1} * (\text{hyd. atoms in inc.})_{T_1} \right] = \text{new D atoms in inc.}$$

$$(\text{hyd. atoms in inc.})_{T_2} \approx (\text{hyd. atoms in inc.})_{T_1}$$

$$\left[ \left( \frac{D}{H} \right)_{T_2} - \left( \frac{D}{H} \right)_{T_1} \right] * (\text{hyd. atoms in inc.})_{T_1} = \text{new D atoms in inc.} = D_{new}$$

271  $D_{new}$  was multiplied by four given the 1:3 D:H stoichiometry of the  $\text{CH}_3\text{D}$  substrate to derive the  
 272 maximum number of methane molecules consumed catabolically through initial C-X bond  
 273 activation (equation 3).

$$D_{new} * 4 = \text{maximum number of methane molecules consumed} = C$$

274 The scaling factor of four was used in the context of methane activation – the initial mobilization  
 275 through conversion to a methyl group – to calculate the maximum number of methane molecules  
 276 that could be consumed but not necessarily fully oxidized. This represents an end-member case  
 277 that may not be appropriate for all subsequent processing as hydrogen/deuterium atoms are  
 278 incorporated into biomass or exchanged. Caveats and potential interpretations of the absolute  
 279 numbers that result from these calculations are discussed below, but we stress that with consistent  
 280 implementation of scaling factors from comparisons between monodeuterated and radiolabel  
 281 methods, rates derived from  $C$  and downstream parameters are valid and useful.

282  $C$  was corrected based on the fraction of incubation methane headspace composed of  
 283  $\text{CH}_3\text{D}$ , yielding  $C_{corr}$ , as shown in equation 4:

$$\frac{C}{\text{fraction of methane headspace that is } \text{CH}_3\text{D}} = C_{corr}$$

284 By dividing  $C_{corr}$  by the incubation time and volume, a maximum rate of methane consumption is  
 285 determined (equation 5.1-5.2):

$$C_{corr} * \frac{\text{mol}}{6.022 \times 10^{23} \text{ molecules}} * \frac{10^9 \text{ nmol}}{\text{mol}} * \frac{1}{\text{incubation time (d)}} * \frac{1}{\text{incubation vol (cm}^3\text{)}} = R_{\text{CH}_3\text{D}}$$

$$R_{\text{CH}_3\text{D}} = \text{Maximum rate of methane consumption in } \frac{\text{nmol}}{\text{cm}^3 \text{ d}}$$

### 286 2.2.2. Rate Measurements Derived from $^{14}\text{CH}_4$ Addition

287 Methane oxidation rates using radiolabeled methane substrate were measured as described  
 288 in detail by Treude et al. (2005) and Treude and Ziebis (2010). Radiolabeled methane ( $^{14}\text{CH}_4$   
 289 dissolved in seawater, corresponding to an activity of 13 kBq for culture experiments and 52 kBq  
 290 in sediment and carbonate samples) was injected into each sample container, and samples were  
 291 incubated at the appropriate temperatures for the designated amount of time (see above). To stop  
 292 microbial activity and begin analysis, 2.5 ml of 2.5% NaOH was injected. Sample headspace was

293 flowed through a  $\text{Cu}^{2+}$  oxide-filled 850 °C quartz tube furnace, combusting unreacted  $^{14}\text{CH}_4$  to  
294  $^{14}\text{CO}_2$ . This  $^{14}\text{CO}_2$  was collected in two scintillation vials (23 ml volume) pre-filled with 7 ml  
295 phenylethylamine and 1 ml 2-methoxyethanol, to which 10 ml of scintillation cocktail (Ultima  
296 Gold XR, PerkinElmer) was added. After a 24-hour incubation period, radioactivity from  $^{14}\text{CO}_2$   
297 was measured by scintillation counting (Beckman Coulter LS 6500 Multi-Purpose Scintillation  
298 Counter, 10 minute analysis per sample).

299 Labeled  $^{14}\text{C}$ -inorganic carbon produced during the incubation was quantified as follows.  
300 The entire volume of each incubation sample was transferred into a 250-ml Erlenmeyer flask along  
301 with 1 drop of antifoam and 5 ml of 6M HCl. The flask was immediately stoppered and sealed  
302 with two clamps and parafilm wrapping to prevent gas escape, and placed on a shaking table (60  
303 rpm, room temperature, 24 hours). To collect  $^{14}\text{CO}_2$  generated by the acidification process, a 7-ml  
304 scintillation vial was pre-filled with 1 ml of 2.5% NaOH and 1 ml of phenylethylamine and  
305 suspended from the rubber stopper inside the flask. After the shaking / acidification step, 5 ml of  
306 scintillation cocktail was added, and the vial was measured by scintillation counting after 24 hours.  
307 This method has been demonstrated to recover 98% of  $^{14}\text{CO}_2$  on average (Treude et al., 2003).

308 Finally, sterilized control samples (#10, see Table S1) were set aside after  $^{14}\text{CH}_4$  addition  
309 for gas chromatography to determine the initial concentration of methane gas. 400  $\mu\text{l}$  of headspace  
310 was injected into a gas chromatograph (Shimadzu GC-2014), equipped with a packed stainless  
311 steel Supelco Custom Column (50/50 mixture, 80/100 Porapak N support, 80/100 Porapak Q  
312 column, 6 ft x 1/8 in) and a flame ionization detector. The carrier gas was helium at a flow rate of  
313  $30 \text{ ml min}^{-1}$ , and the column temperature was 60 °C. Results were scaled based on comparison  
314 with standards of known methane concentrations (10 and 100 ppm; Matheson Tri-Gas, Twinsburg,  
315 OH). The rate of methane oxidation was determined by equation 6:

316 
$$\text{Methane Oxidation} = \frac{{}^{14}\text{CO}_2 \cdot \text{CH}_4}{({}^{14}\text{CH}_4 + {}^{14}\text{CO}_2) \cdot v \cdot t}$$

317 in which  ${}^{14}\text{CH}_4$  is the combusted unreacted radiolabeled methane,  ${}^{14}\text{CO}_2$  represents the quantity of  
318 acidified oxidation product,  $\text{CH}_4$  signifies the initial quantity of methane in the experiment,  $v$  is the  
319 volume of sediment or carbonate rock, and  $t$  is the time over which the incubation was active.

### 320 2.2.3. Isotopic Analysis of Methane in the Headspace

321 The methane headspace was analyzed via  ${}^1\text{H}$ -NMR spectroscopy using a Varian 400 MHz  
322 Spectrometer with a broadband auto-tune OneProbe. 300  $\mu\text{l}$  of headspace was passed through  
323  $\text{CDCl}_3$  with a fine needle to absorb the methane.  ${}^1\text{H}$ -NMR spectra were acquired at 298 K without  
324 spinning, using a repetition rate of 10 s to ensure reliable quantification. The spectra were  
325 simulated with the iNMR 4.1.7 software for the determination of the fractional abundances of the  
326  ${}^{12}\text{CH}_4$ ,  ${}^{12}\text{CH}_3\text{D}$ ,  ${}^{13}\text{CH}_4$  and  ${}^{13}\text{CH}_3\text{D}$  isotopologs.

327

## 328 3. Results and Discussion

### 329 3.1. Comparison of $\text{CH}_3\text{D}$ and ${}^{14}\text{CH}_4$ Rate Measurements in Aerobic Methanotroph Cultures

330 D/H ratios were acquired and corresponding  $C_{corr}$  values were calculated at eight points  
331 during the *M. trichosporium* growth curve and seven points of the *M. sedimenti* growth curve.  
332 Three measurements of  ${}^{14}\text{C}$  distributions were acquired for each strain, targeting exponential and  
333 stationary phases (Fig. 1). The Type II alphaproteobacterial methanotroph *M. trichosporium*  
334 exhibited methane consumption rates more than an order of magnitude greater than those of *M.*  
335 *sedimenti* (gammaproteobacterial Type I methanotroph), yet the scaling factor relating the  $\text{CH}_3\text{D}$ -  
336 and  ${}^{14}\text{CH}_4$ -derived rates was remarkably consistent in both cases. Scaling factors were calculated  
337 for both exponential growth and stationary phase, using data points from both  $\text{CH}_3\text{D}$  and  ${}^{14}\text{CH}_4$   
338 experiments. For example, the *M. trichosporium* rate value calculated from  $\text{CH}_3\text{D}$  experimental



339 treatment point (47.5 hours,  $4.16 \times 10^4$  nmol methane consumed) was compared with the rate  
340 determined from  $^{14}\text{CH}_4$  experimental treatment point (47.5 hours,  $2.77 \times 10^4$  nmol methane  
341 consumed), yielding a scaling factor of 1.5 for exponential phase growth. Similarly, data from (140  
342 h,  $5.27 \times 10^4$  nmol,  $\text{CH}_3\text{D}$ ) and (166.5 h,  $4.24 \times 10^4$  nmol,  $^{14}\text{CH}_4$ ) were used for *M. trichosporium*'s  
343 stationary phase scaling factor. Equivalent values were determined for *M. sedimenti* using the  
344 following data points: (140 h,  $7.07 \times 10^3$  nmol,  $\text{CH}_3\text{D}$ ) and (102 h,  $3.43 \times 10^3$  nmol,  $^{14}\text{CH}_4$ ) for the  
345 exponential growth phase, and (476 h,  $7.53 \times 10^3$  nmol,  $\text{CH}_3\text{D}$ ) and (432 h,  $4.30 \times 10^3$  nmol,  
346  $^{14}\text{CH}_4$ ) for stationary phase.

347 In this way, the ratio of methane consumption rates derived from the  $\text{CH}_3\text{D}$  method (using  
348 equations 1-5) and the  $^{14}\text{CH}_4$  method (using equation 6) can be compared. This value is hereafter  
349 referred to as the “D: $^{14}\text{C}$  tracer ratio”. This ratio can be used to evaluate the consistency of the  
350 monodeuterated methane method compared with the well-established  $^{14}\text{CH}_4$  approach, and as an  
351 investigatory tool in catabolic / anabolic processing of methane (see “Understanding the D: $^{14}\text{C}$   
352 Tracer Ratio”, below).

353 D: $^{14}\text{C}$  tracer ratio values were calculated for aerobic methanotroph cultures using the data  
354 specified above and are shown in Table 2; their consistency is a promising indicator of the utility  
355 of the monodeuterated methane approach for ground-truthed rate measurements. By dividing rates  
356 derived from D/H values by 1.5, a reliable estimate of full-oxidation methanotrophy – that is, the  
357 complete biological oxidation of methane to carbon dioxide – can be assessed.

### 358 3.2. Comparison of $\text{CH}_3\text{D}$ and $^{14}\text{CH}_4$ Rate Measurements in Environmental Methane Seep Samples

359 Methane consumption rates under oxic microcosm incubation conditions, derived from  
360 both  $\text{CH}_3\text{D}$  and  $^{14}\text{CH}_4$  measurements, are provided for all five sample types (active sediment, low-  
361 activity sediment, active porous carbonate, active massive carbonate, and low-activity massive

362 carbonate) in Fig. 2a. The corresponding values for anoxic conditions are shown in Fig. 2b. Values  
363 were calculated from data collected after 4 days of incubation for oxic samples and after 8 days of  
364 incubation for anoxic samples.

365 The D:<sup>14</sup>C tracer ratio for the oxic incubations was 1.66 +/- 0.02 SE and 1.99 +/- 0.04 SE  
366 for anoxic conditions (Table 2). These relatively consistent values across physical substrate type  
367 (sediment and carbonates of varying lithology) and collection site activity level (active and low-  
368 activity) suggest an underlying metabolic basis of these D:<sup>14</sup>C tracer ratio that is unperturbed by  
369 physicochemical factors or relative activity levels.

370 To determine the minimum number of activated CH<sub>3</sub>D molecules needed for analytical  
371 detection, we assessed the length of time required to measure a differentiable D/H ratio.  
372 Measurements were acquired at multiple time points between days 20 and 22 of a triplicate set of  
373 A.Sed-5128 incubations. A resolvable signal of an enhanced D/H ratio was defined as data points  
374 with non-overlapping confidence intervals, representing a 95% statistical probability that D/H  
375 ratios were increased. Such differentiation seen at the 20-hour sampling time for two replicates and  
376 the 26-hour sampling time for the other one (Fig. S1). Using the rate determined by the first 20  
377 days as a baseline, this translates to a resolution of 4.5-6.2 μmol of fully oxidized methane based  
378 on the D:<sup>14</sup>C tracer ratio of 2.05 (Table 2).

### 379 3.3. Understanding the D:<sup>14</sup>C Tracer Ratio

380 The CH<sub>3</sub>D and <sup>14</sup>CH<sub>4</sub> approaches quantify distinct aspects of methanotrophy; that is,  
381 methane activation or complete conversion to CO<sub>2</sub>, respectively. The <sup>14</sup>CH<sub>4</sub> technique quantifies  
382 the amount of <sup>14</sup>C – initially supplied as methane – that is fully oxidized and persists as soluble  
383 species (HCO<sub>3</sub><sup>-</sup>) or acid-labile precipitation products (CaCO<sub>3</sub>). The CH<sub>3</sub>D protocol, on the other  
384 hand, reports the extent to which methane-derived hydrogen atoms are detected in water. Because

385 methane is an inert molecule, abiotic exchange between methane- and water-associated hydrogen  
386 atoms is not expected. Indeed, D/H ratios in killed control experiments remained stable (e.g.,  
387 exhibiting a value of  $1.40 \times 10^{-4} \pm 3.1 \times 10^{-8}$  SE at  $T_{0d}$  and  $1.40 \times 10^{-4} \pm 2.9 \times 10^{-8}$  SE at  $T_{140d}$   
388 during experimentation with *M. trichosporium*, data incorporated into Fig. 1a). The activation of  
389 methane thereby indicates enzymatic functionalization, but the ultimate fate of each hydrogen atom  
390 during methane oxidation is unclear.

391 The flow of methane-derived hydrogen atoms through anaerobic and aerobic  
392 methanotrophic metabolisms was examined in an attempt to predictively evaluate the consequence  
393 of monodeuterated methane reactions. Previously published reports were used to compile Figure 3  
394 (Hallam et al., 2004; Thauer, 2011; Vorholt and Thauer, 1997) and Figure 4 (Lieberman and  
395 Rosenzweig, 2004), which trace anaerobic and aerobic methane metabolisms, respectively, with a  
396 specific focus on hydrogen atoms. In this context, our observations of relatively consistent but  
397 distinct D:<sup>14</sup>C tracer ratios for anaerobic and aerobic methanotrophy (Table 2) likely reflect  
398 different aspects of the two metabolic pathways. In AOM, metabolite backflux (Holler et al., 2011)  
399 may increase the D/H ratio; in aerobic methanotrophy, biomass growth represents a substantial  
400 carbon and hydrogen shunt.

### 401 3.3.1. The D:<sup>14</sup>C Tracer Ratio in Anaerobic Methanotrophy

402 AOM is depicted in Fig. 3 via the reverse methanogenesis pathway, which is believed to be  
403 enacted by ANME based on genetic (Hallam et al., 2004) and proteomic (Marlow et al., 2016)  
404 data. In this metabolic process, methyl-coenzyme M reductase (Mcr) activates methane and  
405 generates methyl-CoM. A tetrahydromethanopterin molecule supplants CoM, and subsequent  
406 carbon oxidation steps release hydrogen atoms into the medium. Ultimately, the number of  
407 methane-derived hydrogen atoms that enter water-exchangeable products determines the

408 physiological interpretation of aqueous D/H ratios. For example, if just one methane-derived  
409 hydrogen enters an intermediate and is freely exchangeable with water, then observed water-based  
410 deuterium must be multiplied by four (to account for methane's hydrogen-carbon stoichiometry;  
411 see equation 3) and a primary isotope effect as high as 2.44 (*M. marburgensis*' Mcr's C-H vs. C-D  
412 bond-breaking preference, Scheller et al., 2013) to arrive at the actual quantity of activated  
413 methane molecules. In this context, the experimental D:<sup>14</sup>C tracer ratio values may provide useful  
414 insight. A D:<sup>14</sup>C tracer ratio of 2 for the reverse methanogenesis pathway suggests that, for every  
415 methane molecule that is fully oxidized to CO<sub>2</sub>, two hydrogen atoms enter water-exchangeable  
416 intermediates.

417         However, the back reaction of enzymatic processes (Scheller et al., 2010) could lead to  
418 heightened D/H ratios in the absence of full carbon oxidation. For example, upon the activation of  
419 methane by Mcr, HS-CoB and CH<sub>3</sub>-S-CoM form, with the thiol hydrogen exchanging with water-  
420 bound hydrogen. If the S-bound hydrogen were deuterium, then the methane re-formed by Mcr  
421 back reaction would be CH<sub>4</sub> and the aqueous deuterium would cause a heightened D/H ratio  
422 despite a lack of net methane oxidation (Fig. 3). We analyzed the remaining headspace of seep  
423 sediment incubations for the formation of CH<sub>4</sub> from CH<sub>3</sub>D via <sup>1</sup>H-NMR spectroscopy. Over the  
424 course of 58 days in triplicate A.Sed-5128 incubations prepared with exclusively CH<sub>3</sub>D headspace,  
425 CH<sub>4</sub> in the headspace increased from 0.33% +/- 0.02% SE to 4.48% +/- 0.27% SE. If this  
426 demonstrated reversibility only reflects the back reaction of Mcr, then the CH<sub>4</sub> increase must be  
427 multiplied by four to reflect the actual percentage of headspace methane that was re-formed by  
428 Mcr; if the reversibility reflects back reaction of the entire pathway, then no scaling factor is  
429 needed. Thus, the range of potential methane headspace percentage accounted for by methane  
430 reformed from initial CH<sub>3</sub>D is between 4.15 – 16.6%. (For clarity, these calculations neglect

431 isotope effects and activity by methanogens, factors that can be clarified through further  
432 experimentation.) Reversibility can be evaluated in future stable isotope work by a) including a  
433  $^{13}\text{C}$ -dissolved inorganic carbon (DIC) signal in the water and measuring  $^{13}\text{CH}_4$ , and/or b) utilizing  
434 multiply deuterated methane as initial headspace and quantifying all possible isotopologs.  
435 Nonetheless, even the upper bound of partially and reversibly oxidized  $\text{CH}_3\text{D}$  suggests that the  
436 majority of the D/H signal is attributable to reactions indicative of net methane consumption, if not  
437 complete oxidation.

### 438 3.3.2. The D: $^{14}\text{C}$ Tracer Ratio in Aerobic Methanotrophy

439 In aerobic methanotrophic cultures, a D: $^{14}\text{C}$  tracer ratio of  $\sim 1.5$  was observed, suggesting  
440 that on average, 2.67 of the four methane-derived hydrogen atoms likely enter water-exchangeable  
441 products during the course of a full oxidation pathway. *M. tricosporium* is a type II methanotroph,  
442 a member of the *Alphaproteobacteria* that uses the serine pathway for carbon assimilation; *M.*  
443 *sedimenti* is a gammaproteobacterial type I methanotroph, using the RuMP carbon assimilation  
444 pathway (Tavormina et al., 2015). The pathway data presented in Fig. 4 suggests that all methane-  
445 bound hydrogens are water exchangeable during the catabolic oxidation of methane to carbon  
446 dioxide. Thus, to achieve a D: $^{14}\text{C}$  tracer ratio less than 4, a substantial proportion of methane-  
447 derived formaldehyde would need to proceed down the assimilatory pathway, a requirement that  
448 was likely met given the cultures' increase in cell density (data not shown). Intriguingly, the D: $^{14}\text{C}$   
449 tracer ratios were similar for both cultured organisms despite their distinct metabolic pathways; a  
450 similar phenomenon of consistent carbon conversion efficiency was recently observed among  
451 distinct aerobic methanotroph communities in English riverbeds (Trimmer et al., 2015).

452 The oxic incubations of methane seep sediment produced a D: $^{14}\text{C}$  tracer ratio of  $1.66 \pm$   
453  $0.02$  SE. Given that the known modes of biological methane oxidation – type I and type II aerobic

454 methanotrophy and reverse methanogenesis anaerobic methanotrophy – bound this observed value,  
455 it appears likely that the oxic sediment incubations supported a mixture of both aerobic and  
456 anaerobic methane oxidation processes. Aerobic methane oxidation likely dominated, based on the  
457  $\sim 7 \times 10^4$  Pa partial pressure of  $O_2$  and the proximity of the D: $^{14}C$  tracer ratio to that of the aerobic  
458 methanotrophic cultures, but anoxic niches likely remained or developed in the incubation bottles.

#### 459 3.4. Specialized Application of the Monodeuterated Methane Approach: Anaerobic Methanotrophy 460 at Pressure

461 To demonstrate the utility of the  $CH_3D$  rate measurement approach in addressing  
462 experimentally relevant questions, particularly in nontraditional empirical contexts, we sought to  
463 evaluate the influence of *in situ* pressure on methanotrophic rates of Hydrate Ridge seep sediment  
464 microbial communities. Material collected for microbiological studies of AOM is frequently  
465 obtained from marine settings of various depths that are subjected to distinct and substantial  
466 pressure regimes (Ruff et al., 2015). Pressure is not always rigorously incorporated into microcosm  
467 experiments, though evidence suggests it can be an important determinant of methanotrophic rates  
468 (Bowles et al., 2011; Nauhaus et al., 2005; Zhang et al., 2010). In addition, some procedural  
469 aspects of the  $^{14}CH_4$  protocol, including headspace sampling and full-volume transfer, are not  
470 established for use with mylar bags, making the monodeuterated methane approach an appealing  
471 alternative in this context.

472 Parallel seep sediment incubations were subjected to 0.1 MPa (atmospheric pressure) and  
473 9.0 MPa (equivalent to  $\sim 900$  m depth).  $\delta D$  values derived from heightened D/H ratios attributable  
474 to methane consumption, are shown in Fig. 5. A significant increase in methane consumption was  
475 observed in both live conditions at heightened pressure, corresponding to sediment incubated with  
476 glycine (samples 1a and 1b) and ammonium chloride (samples 2a and 2b). Controls lacking  $CH_3D$

477 (samples 3a and 3b) and biological activity (samples 4a and 4b) showed no increase in  $\delta D$  (see  
478 Table S2 for sample set-up details). The simulation of *in situ* Hydrate Ridge pressures led to a  
479 79.5% (+/- 6.5 SE) increase in relative methane oxidizing rates. Incubation with 500  $\mu M$  glycine  
480 rather than ammonium at high and low pressures resulted in small but consistent rate increases of  
481 12% +/- 4.1% SE, potentially reflecting the energetic and biosynthetic distinction between  
482 exogenous amino acids and unprocessed fixed nitrogen.

483         Previous reports have found a wide range of different pressure-related effects. In a sulfate-  
484 coupled AOM bioreactor, pressures were varied from 1 to 8 MPa and sulfide production  
485 approximately tripled, demonstrating Michaelis-Menten style kinetics with an apparent  $K_m$  of 37  
486 mM (Zhang et al., 2010). Methane partial pressures of 1.1 MPa led to a 5x increase in sulfate  
487 reduction rates relative to ambient atmospheric pressure with Hydrate Ridge sediments  
488 demonstrating methane-dependent sulfate reduction (Nauhaus et al., 2002). With methane seep  
489 sediment from the Japan Trench, however, methane-driven sulfate reduction rates did not correlate  
490 with changing pressure (Vossmeyer et al., 2012). Nauhaus et al. (2005) suggested that the pressure-  
491 induced rate increases are due more to heightened methane solubility and bioavailability rather  
492 than physiological effects or biomolecular re-ordering. Bowles et al. (2011) presented a very  
493 different perspective by showing a six- to ten-fold AOM rate increase at 10 MPa when methane  
494 concentrations were held constant. Deconvolving these two influences and how they depend on  
495 community composition or physicochemical parameters is feasible with pressure chamber  
496 experiments utilizing monodeuterated methane. Understanding the relative contributions of  
497 environmental and physiological effects to methane oxidation will help constrain methane fluxes  
498 across a larger envelope of the planet's methanotrophically active zones.

### 499 3.5. Using Monodeuterated Methane in Experimental Investigations

500 Based on  $^{14}\text{CH}_4$  ground-truthing experiments with aerobic methanotrophic cultures, oxic  
501 seep sediment, and anoxic seep sediment, as well as the proof-of-concept pressurized experiments,  
502 we believe that the monodeuterated methane approach to methane oxidation rate measurement is a  
503 useful addition to the biogeochemist's tool set. Compared with radiolabel approaches ( $^{14}\text{CH}_4$ ,  $^3\text{H}$ -  
504  $\text{CH}_4$ ,  $^{35}\text{SO}_4^{2-}$ ), the method requires less safety-oriented planning, and is logistically simpler, more  
505 affordable, and may be less susceptible to hydrogen-associated isotope fractionation effects  
506 (relative to  $^3\text{H}$ ). Our results also suggest that the monodeuterated methane technique appears to be  
507 a more precise method based on standard error calculations (Figs. 1, 2). Direct comparisons of  
508 environmental incubations are complicated by the microheterogeneity of seep settings (Barry et al.,  
509 1996; Lloyd et al., 2010), as well as the fact that different aliquots of the same initial material were  
510 used in our experiments. However, analysis of culture-based experiments reveals that standard  
511 errors from  $R_{\text{CH}_3\text{D}}$  values were 20% those derived from  $^{14}\text{CH}_4$ -based values, making the  
512 monodeuterated method five times more precise.

513 Because the monodeuterated methane method focuses on methane-bound hydrogen atoms,  
514 it offers different, complementary information about methanotrophic systems than carbon-based  
515 techniques like methane or bicarbonate quantification. While this distinction complicates the  
516 interpretation of isolated D/H ratios, it can offer an additional dimension of information for  
517 analysis of methane-derived intermediates in relevant metabolisms. Given these caveats, we  
518 recommend three use cases for monodeuterated methane in methane oxidation rate measurement  
519 applications.

520 1) First, the approach can be employed in a strictly comparative context using analogous  
521 inoculum exposed to a range of different conditions, as demonstrated with the pressure-  
522 based sediment incubations presented above. Evaluating the effect of different



523 conditions such as temperature ranges, chemical concentrations, or energetic landscapes  
524 on seep sediment methane oxidizing rates would all be promising applications.  
525 Comparative analysis of AOM rates at different seep sites would also be useful,  
526 provided anaerobic or aerobic methanotrophic processes could be isolated.

527 2) Second, by performing side-by-side monodeuterated methane and radiocarbon tests, a  
528 sample-specific D:<sup>14</sup>C tracer ratio can be determined, and absolute rates of full methane  
529 oxidation can then be inferred in subsequent experiments based exclusively on D/H  
530 ratios. Conducting such paired studies under additional environmental or lab-based  
531 conditions would help clarify the universality of the ratios presented here and would  
532 likely reveal additional questions of metabolic dynamics in a range of experimental  
533 systems. We also encourage side-by-side comparisons with other rate measurement  
534 approaches, including <sup>3</sup>H-CH<sub>4</sub> radiotracer and methane concentration assessments, to  
535 develop additional pairwise conversion factors and better constrain carbon and hydrogen  
536 metabolism in methane-based biological reactions.

537 3) Finally, the use of monodeuterated methane as an analytical tool, alongside additional  
538 methods such as carbon- or sulfur-tracking procedures, would enable a multi-  
539 dimensional examination of anabolic and catabolic processes in methane-based  
540 metabolisms. In particular, the D:<sup>14</sup>C tracer ratios presented here reveal intriguing and  
541 seemingly systematic relationships between carbon and hydrogen anabolic and catabolic  
542 partitioning across distinct physiologies, yet an underlying theoretical framework  
543 regarding the fate of methane-bound hydrogen atoms remains outstanding. In anaerobic  
544 methanotrophic systems, back-reaction rates and equilibrium constants could be  
545 evaluated by a) including a <sup>13</sup>CO<sub>2</sub> signal in the water and measuring <sup>13</sup>CH<sub>4</sub>, and/or b)

546 utilizing multiply deuterated methane as initial headspace and measuring all possible  
547 isotopologues via NMR or high resolution mass spectrometry. For aerobic  
548 methanotrophs, evaluating D:<sup>14</sup>C tracer ratios under more clearly defined growth and  
549 maintenance phases would elucidate distinct values associated with catabolic, RuMP,  
550 and serine pathways, enabling future use of that parameter as an arbiter of relative  
551 anabolic and catabolic activity. Furthermore, additional environmental variables can be  
552 tested to gain insight into distinct redox pathways and dynamics of reversibility. For  
553 example, AOM under lower sulfate concentrations might be expected to generate higher  
554 D:<sup>14</sup>C tracer ratios (Yoshinaga et al., 2014), and this parameter could be further  
555 developed as a measure of microbially mediated isotopic equilibration.

556

#### 557 **4. Conclusion**

558 The ability to accurately measure methane consumption and oxidation rates – both  
559 comparatively and in absolute values – is an important component of methanotrophic studies. Such  
560 measurements frequently depend on radiotracers or measurements of chemical species that are  
561 related to, but not directly indicative of, methane metabolism. The monodeuterated methane  
562 technique presented here represents a novel approach to methane oxidation rate measurements,  
563 notable for its logistical and analytical ease (particularly in ship-board applications), as well as the  
564 added dimension provided by H-based, rather than C-based, information. We have demonstrated  
565 that the D/H ratio is a reliable proxy for methane oxidation activity: in several applications, the  
566 value is directly proportional to methane oxidation rates as measured in absolute terms by the well-  
567 established <sup>14</sup>CH<sub>4</sub> method. The value of the proportionality constant differs based on the  
568 experimental system, likely dictated by environmental variables and the relative proportions of

569 aerobic and anaerobic methanotrophic metabolisms, though additional experiments to determine  
570 the nature of the putative mixing line are needed.

571 Methane biogeochemistry is a dynamic field of study with implications for carbon cycling,  
572 microbial ecology, and climate dynamics, though experimental challenges have slowed our  
573 understanding of methane-based biological reactions. With the CH<sub>3</sub>D approach as an added tool in  
574 the arsenal of rate-based examinations, a broader understanding of the intricacies of methane  
575 metabolism, as well as its role in environmental and anthropogenic systems, is within reach.

576

## 577 **5. Acknowledgements**

578 We thank the Captains, Crew, *Alvin* group, *Jason* group, and Science party members from  
579 *RV Atlantis* legs AT-15-68, and AT-18-10. Water analyzer measurements were conducted in the  
580 laboratory of Alex Sessions at the California Institute of Technology with technical support from  
581 Lichun Zhang. We are indebted to William Berelson at the University of Southern California and  
582 Nick Rollins for use of their pressure chambers and assistance with the incubation experiments.  
583 We thank Alex Sessions, Woodward Fischer, Dianne Newman, Tori Hoehler, Amy Rosenzweig,  
584 Daniel Stolper, and Linda Reynard for helpful conversations during the preparation of the  
585 manuscript. This study was funded by grants from the U.S. Department of Energy, Office of  
586 Science, Office of Biological and Environmental Research (DE-SC001057), the NASA  
587 Astrobiology Institute (Award # NNA13AA92A) and support from the Gordon and Betty Moore  
588 Foundation through grant GBMF3780 (to VJO). JJM was supported by a National Energy  
589 Technology Laboratory Methane Hydrate Research Fellowship funded by the National Research  
590 Council of the National Academies. This research used resources of the Oak Ridge Leadership

591 Computing Facility. Oak Ridge National Laboratory is supported by the Office of Science of the  
592 U.S. Department of Energy.

593

## 594 **6. References**

595 Alperin, M. J., and Reeburgh, W. S. (1985). Inhibition Experiments on Anaerobic Methane Oxidation.  
596 *Applied and Environmental Microbiology* 50, 940–945.

597 Barry, J. P., Gary Greene, H., Orange, D. L., Baxter, C. H., Robison, B. H., Kochevar, R. E., et al.  
598 (1996). Biologic and geologic characteristics of cold seeps in Monterey Bay, California. *Deep Sea*  
599 *Research Part I: Oceanographic Research Papers* 43, 1739–1762.

600 Beal, E. J., House, C. H., and Orphan, V. J. (2009). Manganese- and Iron-Dependent Marine Methane  
601 Oxidation. *Science* 325, 184–187. doi:10.1126/science.1169984.

602 Boetius, A., Ravensschlag, K., Schubert, C. J., Rickert, D., Widdel, F., Gleseke, A., et al. (2000). A  
603 marine microbial consortium apparently mediating anaerobic oxidation of methane. *Nature*  
604 407.

605 Boetius, A., and Suess, E. (2004). Hydrate Ridge: a natural laboratory for the study of microbial life  
606 fueled by methane from near-surface gas hydrates. *Chemical Geology* 205, 291–310.  
607 doi:10.1016/j.chemgeo.2003.12.034.

608 Bowles, M. W., Samarkin, V. A., and Joye, S. B. (2011). Improved measurement of microbial activity in  
609 deep-sea sediments at in situ pressure and methane concentration. *Limnology and Oceanography:*  
610 *Methods* 9, 499–506.

611 Bussmann, I., Matousu, A., Osudar, R., and Mau, S. (2015). Assessment of the radio  $^3\text{H}$ -CH<sub>4</sub> tracer  
612 technique to measure aerobic methane oxidation in the water column. *Limnology and*  
613 *Oceanography: Methods* 13, 312–327.

614 Carini, S. A., Orcutt, B. N., and Joye, S. B. (2003). Interactions between methane oxidation and  
615 nitrification in coastal sediments. *Geomicrobiology Journal* 20, 355–374.

616 Crespo-Medina, M., Meile, C., Hunter, K., Diercks, A., Asper, V., Orphan, V., et al. (2014). The rise  
617 and fall of methanotrophy following a deepwater oil-well blowout. *Nature Geoscience*.

618 Dawson, K., Osburn, M., Sessions, A., and Orphan, V. (2015). Metabolic associations with archaea  
619 drive shifts in hydrogen isotope fractionation in sulfate-reducing bacterial lipids in cocultures  
620 and methane seeps. *Geobiology* 13, 462–477.

621 Dunfield, P. F., Yuryev, A., Senin, P., Smirnova, A. V., Stott, M. B., Hou, S., et al. (2007). Methane  
622 oxidation by an extremely acidophilic bacterium of the phylum Verrucomicrobia. *Nature* 450,  
623 879–882.

- 624 Ettwig, K. F., Butler, M. K., Le Paslier, D., Pelletier, E., Mangenot, S., Kuypers, M. M., et al. (2010).  
625 Nitrite-driven anaerobic methane oxidation by oxygenic bacteria. *Nature* 464, 543–548.
- 626 Gieskes, J., Mahn, C., Day, S., Martin, J. B., Greinert, J., Rathburn, T., et al. (2005). A study of the  
627 chemistry of pore fluids and authigenic carbonates in methane seep environments: Kodiak  
628 Trench, Hydrate Ridge, Monterey Bay, and Eel River Basin. *Chemical Geology* 220, 329–345.  
629 doi:10.1016/j.chemgeo.2005.04.002.
- 630 Girguis, P. R., Orphan, V. J., Hallam, S. J., and DeLong, E. F. (2003). Growth and Methane Oxidation  
631 Rates of Anaerobic Methanotrophic Archaea in a Continuous-Flow Bioreactor. *Applied and  
632 Environmental Microbiology* 69, 5472–5482. doi:10.1128/AEM.69.9.5472-5482.2003.
- 633 Hakemian, A. S., and Rosenzweig, A. C. (2007). The biochemistry of methane oxidation. *Annu. Rev.  
634 Biochem.* 76, 223–241.
- 635 Hallam, S. J., Putnam, N., Preston, C. M., Detter, J. C., Rokhsar, D., Richardson, P. M., et al. (2004).  
636 Reverse methanogenesis: testing the hypothesis with environmental genomics. *Science* 305,  
637 1457–1462.
- 638 Haroon, M. F., Hu, S., Shi, Y., Imelfort, M., Keller, J., Hugenholtz, P., et al. (2013). Anaerobic  
639 oxidation of methane coupled to nitrate reduction in a novel archaeal lineage. *Nature* 500, 567–  
640 570.
- 641 Ho, A., Vlaeminck, S. E., Ettwig, K. F., Schneider, B., Frenzel, P., and Boon, N. (2013). Revisiting  
642 methanotrophic communities in sewage treatment plants. *Applied and environmental microbiology*  
643 79, 2841–2846.
- 644 Holler, T., Wegener, G., Niemann, H., Deusner, C., Ferdelman, T. G., Boetius, A., et al. (2011).  
645 Carbon and sulfur back flux during anaerobic microbial oxidation of methane and coupled  
646 sulfate reduction. *Proceedings of the National Academy of Sciences* 108, E1484–E1490.  
647 doi:10.1073/pnas.1106032108.
- 648 Holzapfel-Pschorn, A., Conrad, R., and Seiler, W. (1985). Production, oxidation and emission of  
649 methane in rice paddies. *FEMS Microbiology Ecology* 1, 343–351.
- 650 Huang, M., Hilderman, J. N., and Barbour, L. (2015). Transport of stable isotopes of water and  
651 sulphate within reclaimed oil sands saline–sodic mine overburden. *Journal of Hydrology* 529,  
652 1550–1561.
- 653 Jørgensen, B. B., Weber, A., and Zopfi, J. (2001). Sulfate reduction and anaerobic methane oxidation  
654 in Black Sea sediments. *Deep Sea Research Part I: Oceanographic Research Papers* 48, 2097–2120.
- 655 Kirschke, S., Bousquet, P., Ciais, P., Saunois, M., Canadell, J. G., Dlugokencky, E. J., et al. (2013).  
656 Three decades of global methane sources and sinks. *Nature Geosci* 6, 813–823.
- 657 Knittel, K., and Boetius, A. (2009). Anaerobic Oxidation of Methane: Progress with an Unknown  
658 Process. *Annu. Rev. Microbiol.* 63, 311–334. doi:10.1146/annurev.micro.61.080706.093130.

- 659 Lieberman, R. L., and Rosenzweig, A. C. (2004). Biological methane oxidation: regulation,  
660 biochemistry, and active site structure of particulate methane monooxygenase. *Critical reviews in*  
661 *biochemistry and molecular biology* 39, 147–164.
- 662 Lis, G., Wassenaar, L., and Hendry, M. (2008). High-precision laser spectroscopy D/H and 18O/16O  
663 measurements of microliter natural water samples. *Analytical Chemistry* 80, 287–293.
- 664 Lloyd, K. G., Albert, D. B., Biddle, J. F., Chanton, J. P., Pizarro, O., and Teske, A. (2010). Spatial  
665 structure and activity of sedimentary microbial communities underlying a Beggiatoa spp. mat  
666 in a Gulf of Mexico hydrocarbon seep. *PLoS One* 5, e8738.
- 667 Mackelprang, R., Waldrop, M. P., DeAngelis, K. M., David, M. M., Chavarria, K. L., Blazewicz, S. J., et  
668 al. (2011). Metagenomic analysis of a permafrost microbial community reveals a rapid response  
669 to thaw. *Nature* 480, 368–371.
- 670 Magen, C., Lapham, L. L., Pohlman, J. W., Marshall, K., Bosman, S., Casso, M., et al. (2014). A simple  
671 headspace equilibration method for measuring dissolved methane. *Limnol. Oceanogr. Methods* 12,  
672 637–650.
- 673 Marlow, J. J., Skennerton, C. T., Li, Z., Chourey, K., Hettich, R. L., Pan, C., et al. (2016). Proteomic  
674 Stable Isotope Probing Reveals Biosynthesis Dynamics of Slow Growing Methane Based  
675 Microbial Communities. *Frontiers in microbiology* 7.
- 676 Marlow, J. J., Steele, J. A., Ziebis, W., Thurber, A. R., Levin, L. A., and Orphan, V. J. (2014).  
677 Carbonate-hosted methanotrophy represents an unrecognized methane sink in the deep sea.  
678 *Nature Communications*.
- 679 Mau, S., Bles, J., Helmke, E., Niemann, H., and Damm, E. (2013). Vertical distribution of methane  
680 oxidation and methanotrophic response to elevated methane concentrations in stratified  
681 waters of the Arctic fjord Storfjorden (Svalbard, Norway). *Biogeosciences* 10, 6267–6278.
- 682 McGlynn, S. E., Chadwick, G. L., Kempes, C. P., and Orphan, V. J. (2015). Single cell activity reveals  
683 direct electron transfer in methanotrophic consortia. *Nature* 526, 531–535.
- 684 Moran, J. J., Beal, E. J., Vrentas, J. M., Orphan, V. J., Freeman, K. H., and House, C. H. (2008). Methyl  
685 sulfides as intermediates in the anaerobic oxidation of methane. *Environmental Microbiology* 10,  
686 162–173. doi:10.1111/j.1462-2920.2007.01441.x.
- 687 Nauhaus, K., Boetius, A., Krüger, M., and Widdel, F. (2002). In vitro demonstration of anaerobic  
688 oxidation of methane coupled to sulphate reduction in sediment from a marine gas hydrate  
689 area. *Environmental Microbiology* 4, 296–305. doi:10.1046/j.1462-2920.2002.00299.x.
- 690 Nauhaus, K., Treude, T., Boetius, A., and Krüger, M. (2005). Environmental regulation of the  
691 anaerobic oxidation of methane: a comparison of ANME-I and ANME-II communities.  
692 *Environmental Microbiology* 7, 98–106. doi:10.1111/j.1462-2920.2004.00669.x.
- 693 Op den Camp, H. J. M., Islam, T., Stott, M. B., Harhangi, H. R., Hynes, A., Schouten, S., et al. (2009).  
694 Environmental, genomic and taxonomic perspectives on methanotrophic Verrucomicrobia.  
695 *Environmental Microbiology Reports* 1, 293–306. doi:10.1111/j.1758-2229.2009.00022.x.

- 696 Pack, M. A., Heintz, M. B., Reeburgh, W. S., Trumbore, S. E., Valentine, D. L., Xu, X., et al. (2011). A  
697 method for measuring methane oxidation rates using low levels of  $^{14}\text{C}$ -labeled methane and  
698 accelerator mass spectrometry. *Limnology and Oceanography: Methods* 9, 245–260.
- 699 Reeburgh, W. S. (2007). Oceanic Methane Biogeochemistry. *Chem. Rev.* 107, 486–513.  
700 doi:10.1021/cr050362v.
- 701 Robson, T., and Webb, J. (2016). The use of environmental tracers to determine focused recharge  
702 from a saline disposal basin and irrigation channels in a semiarid environment in Southeastern  
703 Australia. *Journal of Hydrology* 538, 326–338.
- 704 Ruff, S. E., Biddle, J. F., Teske, A. P., Knittel, K., Boetius, A., and Ramette, A. (2015). Global  
705 dispersion and local diversification of the methane seep microbiome. *Proceedings of the National  
706 Academy of Sciences*, 201421865.
- 707 Ruff, S. E., Kuhfuss, H., Wegener, G., Lott, C., Ramette, A., Wiedling, J., et al. (2016). Methane seep in  
708 shallow-water permeable sediment harbors high diversity of anaerobic methanotrophic  
709 communities, Elba, Italy. *Frontiers in microbiology* 7.
- 710 Scheller, S., Goenrich, M., Boecher, R., Thauer, R. K., and Jaun, B. (2010). The key nickel enzyme of  
711 methanogenesis catalyses the anaerobic oxidation of methane. *Nature* 465, 606–608.
- 712 Scheller, S., Goenrich, M., Thauer, R. K., and Jaun, B. (2013). Methyl-Coenzyme M Reductase from  
713 Methanogenic Archaea: Isotope Effects on the Formation and Anaerobic Oxidation of  
714 Methane. *J. Am. Chem. Soc.* 135, 14975–14984. doi:10.1021/ja406485z.
- 715 Scheller, S., Yu, H., Chadwick, G. L., McGlynn, S. E., and Orphan, V. J. (2016). Artificial electron  
716 acceptors decouple archaeal methane oxidation from sulfate reduction. *Science* 351, 703–707.
- 717 Scheutz, C., Bogner, J., De Visscher, A., Gebert, J., Hilger, H., Huber-Humer, M., et al. (2009).  
718 Microbial methane oxidation processes and technologies for mitigation of landfill gas  
719 emissions. *Waste Management & Research*.
- 720 Segarra, K. E., Comerford, C., Slaughter, J., and Joye, S. B. (2013). Impact of electron acceptor  
721 availability on the anaerobic oxidation of methane in coastal freshwater and brackish wetland  
722 sediments. *Geochimica et Cosmochimica Acta* 115, 15–30.
- 723 Sivan, O., Antler, G., Turchyn, A. V., Marlow, J. J., and Orphan, V. J. (2014). Iron oxides stimulate  
724 sulfate-driven anaerobic methane oxidation in seeps. *Proceedings of the National Academy of Sciences*  
725 111, E4139–E4147. doi:10.1073/pnas.1412269111.
- 726 Suess, E., Torres, M., Bohrmann, G., Collier, R., Greinert, J., Linke, P., et al. (1999). Gas hydrate  
727 destabilization: enhanced dewatering, benthic material turnover and large methane plumes at  
728 the Cascadia convergent margin. *Earth and Planetary Science Letters* 170, 1–15.
- 729 Tavormina, P. L., Hatzenpichler, R., McGlynn, S., Chadwick, G., Dawson, K. S., Connon, S. A., et al.  
730 (2015). *Methyloprofundus sedimenti* gen. nov., sp. nov., an obligate methanotroph from ocean

- 731 sediment belonging to the “deep sea-1” clade of marine methanotrophs. *International journal of*  
732 *systematic and evolutionary microbiology* 65, 251–259.
- 733 Thauer, R. K. (2011). Anaerobic oxidation of methane with sulfate: on the reversibility of the reactions  
734 that are catalyzed by enzymes also involved in methanogenesis from CO<sub>2</sub>. *Current opinion in*  
735 *microbiology* 14, 292–299.
- 736 Treude, Boetius, Knittel, Wallmann, and Jørgensen (2003). Anaerobic oxidation of methane above gas  
737 hydrates at Hydrate Ridge, NE Pacific Ocean. *Mar Ecol Prog Ser* 264, 1–14.
- 738 Treude, T., Krüger, M., Boetius, A., and Jørgensen, B. B. (2005). Environmental control on anaerobic  
739 oxidation of methane in the gassy sediments of Eckernförde Bay (German Baltic). *Limnology*  
740 *and oceanography* 50, 1771–1786.
- 741 Treude, T., and Ziebis, W. (2010). Methane oxidation in permeable sediments at hydrocarbon seeps in  
742 the Santa Barbara Channel, California. *Biogeosciences (BG)* 7, 3095–3108.
- 743 Trimmer, M., Shelley, F. C., Purdy, K. J., Maanoja, S. T., Chronopoulou, P.-M., and Grey, J. (2015).  
744 Riverbed methanotrophy sustained by high carbon conversion efficiency. *ISME J* 9, 2304–  
745 2314.
- 746 Tryon, M. ., Brown, K. ., and Torres, M. . (2002). Fluid and chemical flux in and out of sediments  
747 hosting methane hydrate deposits on Hydrate Ridge, OR, II: Hydrological processes. *Earth and*  
748 *Planetary Science Letters* 201, 541–557. doi:10.1016/S0012-821X(02)00732-X.
- 749 Valentine, D. L., Blanton, D. C., Reeburgh, W. S., and Kastner, M. (2001). Water column methane  
750 oxidation adjacent to an area of active hydrate dissociation, Eel river Basin. *Geochimica et*  
751 *Cosmochimica Acta* 65, 2633–2640. doi:10.1016/S0016-7037(01)00625-1.
- 752 Vorholt, J. A., and Thauer, R. K. (1997). The Active Species of “CO<sub>2</sub>” Utilized by  
753 Formylmethanofuran Dehydrogenase from Methanogenic Archaea. *European Journal of*  
754 *Biochemistry* 248, 919–924. doi:10.1111/j.1432-1033.1997.00919.x.
- 755 Vossmeier, A., Deusner, C., Kato, C., Inagaki, F., and Ferdelman, T. G. (2012). Substrate-specific  
756 pressure-dependence of microbial sulfate reduction in deep-sea cold seep sediments of the  
757 Japan Trench. *Frontiers in Microbiology* 3, 253. doi:10.3389/fmicb.2012.00253.
- 758 Wegener, G., Krukenberg, V., Riedel, D., Tegetmeyer, H. E., and Boetius, A. (2015). Intercellular  
759 wiring enables electron transfer between methanotrophic archaea and bacteria. *Nature* 526,  
760 587–590.
- 761 Whittenbury, R., Phillips, K., and Wilkinson, J. (1970). Enrichment, isolation and some properties of  
762 methane-utilizing bacteria. *Journal of General Microbiology* 61, 205–218.
- 763 Yoshinaga, M. Y., Holler, T., Goldhammer, T., Wegener, G., Pohlman, J. W., Brunner, B., et al. (2014).  
764 Carbon isotope equilibration during sulphate-limited anaerobic oxidation of methane. *Nature*  
765 *Geosci* 7, 190–194.



766 Zhang, Y., Henriot, J.-P., Bursens, J., and Boon, N. (2010). Stimulation of in vitro anaerobic oxidation  
 767 of methane rate in a continuous high-pressure bioreactor. *Bioresource Technology* 101, 3132–3138.  
 768 doi:10.1016/j.biortech.2009.11.103.

769  
 770

771 **7. Tables and Figure Captions**

772 Table 1: A summary of the samples used for all experiments conducted in this study. Green boxes  
 773 indicate that the experiment took place (with all relevant permutations and controls, as described in  
 774 the text); blank boxes indicate experiments that were not conducted. CH<sub>3</sub>D refers to  
 775 methanotrophic rate experiments using the novel monodeuterated methane technique, while <sup>14</sup>CH<sub>4</sub>  
 776 refers to the radiolabel-based experiments. The three-part codes for samples derived from  
 777 environmental material refer to active (A) or low-activity (L) sediments (Sed) or carbonates (Carb),  
 778 along with a sample-specific four-digit serial number.

779

		Oxic		Anoxic	
		CH <sub>3</sub> D	<sup>14</sup> CH <sub>4</sub>	CH <sub>3</sub> D	<sup>14</sup> CH <sub>4</sub>
Aerobic Methanotroph Cultures Experiment					
	<i>M. trichosporium</i>				
	<i>M. sedimenti</i>				
Seep Sediment Experiment					
	A.Sed-5128				
	L.Sed-5043				
Seep Carbonate Experiment					
	A.Carb-5305				
	A.Carb-5152				
	L.Carb-5028				
Pressure Experiment					
	A.Sed-3450				

780  
 781

782 Table 2: D:<sup>14</sup>C tracer ratios for the experimental treatments addressed in this study.

783

<b>Aerobic Methanotroph Cultures</b>		
	Exponential Phase	Stationary Phase
<i>M. trichosporium</i>	1.5	1.48
<i>M. sedimenti</i>	1.54	1.59
<b>Methane Seep Sediments and Carbonates</b>		
	Oxic Incubations	Anoxic Incubations
A.Sed-5128	1.62	2.05
L.Sed-5043	1.71	2.01
A.Carb-5305	1.65	1.96
A.Carb-5152	1.63	2.08
L.Carb-5028	1.69	1.86

784

785

786 Fig. 1: Amount of methane consumed over time for cultures of a) the type II methanotroph *M.*  
787 *trichosporium* and b) the type I methanotroph *M. sedimenti* using  $C_{corr}$  (values derived from the  
788  $\text{CH}_3\text{D}$  method, shown with circles) and the  $^{14}\text{CH}_4$  method (diamonds), calculated as discussed in  
789 the text.  $^{14}\text{CH}_4$ -derived data conveys values of methane consumption and full oxidation, while  
790  $\text{CH}_3\text{D}$ -derived data provides a measure of methane consumption. Error bars show standard errors  
791 for three biological replicates, with the exception of the  $^{14}\text{CH}_4$ -derived killed control (n=1).  
792 Obscured data points exhibited values between -60 and 110 nmol for a) and 0 and 60 nmol for b).

793

794 Fig. 2: Methanotrophy in a) oxic and b) anoxic incubations of active and inactive seep sediment  
795 and carbonate rocks (n=3 in all cases). Values compare methane consumption / full oxidation rates  
796 derived from  $^{14}\text{CH}_4$  measurements (blue) and methane consumption rates derived from the  $\text{CH}_3\text{D}$   
797 approach (green,  $R_{\text{CH}_3\text{D}}$  values). Standard error bars are provided.

798

799 Fig. 3: A schematic diagram demonstrating the potential fate of methane-associated hydrogen  
800 atoms in the “reverse methanogenesis” pathway. Hydrogen atoms are distinguished by color and  
801 superscript number, and potential exchanges with inter- and intra-cellular water are shown.

802 Potentially detectable methane-derived hydrogen atoms (4, occurring throughout the oxidation  
803 pathway) and carbon atoms (1, requiring full oxidation) are highlighted in orange and purple  
804 boxes, respectively. Shorter “backflux” arrows reflect the observation that all enzymes (Thauer,  
805 2008) and the entire pathway (Holler et al., 2011) have been shown to be reversible. For figure  
806 simplicity, isotopically distinct backflux products and cofactor involvement in backflux reactions  
807 are not shown. The extended dashed line represents the cell membrane.

808

809 Fig. 4: A schematic diagram demonstrating the potential fate of methane-associated hydrogen  
810 atoms in the aerobic methanotrophy pathways. Hydrogen atoms are distinguished by color and  
811 superscript number; asterisks represent location-specific ambiguity. Potentially detectable  
812 methane-derived hydrogen atoms and carbon atoms are highlighted in orange and purple boxes,  
813 respectively. Mmo enzymes are not believed to perform reversible reactions.

814

815 Fig. 5: Pressure experiment results showing water  $\delta D$  values with standard error bars of seep  
816 sediment samples following 38-day incubations with  $CH_3D$  at 9.0 MPa (brown bars, “b” samples)  
817 or 0.1 MPa (pink bars, “a” samples). Additional details on sample treatments can be found in Table  
818 S2.

Figure 1

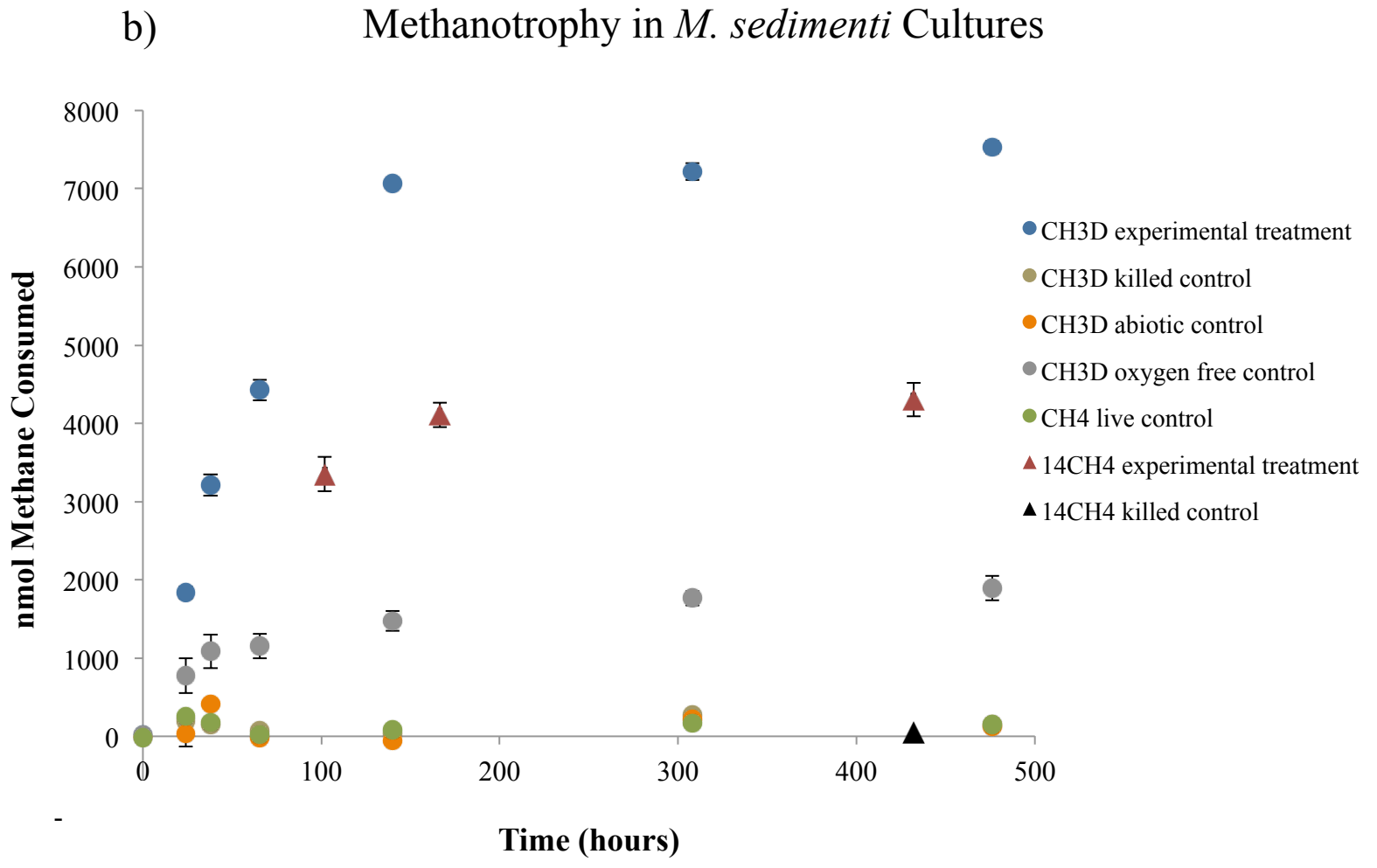
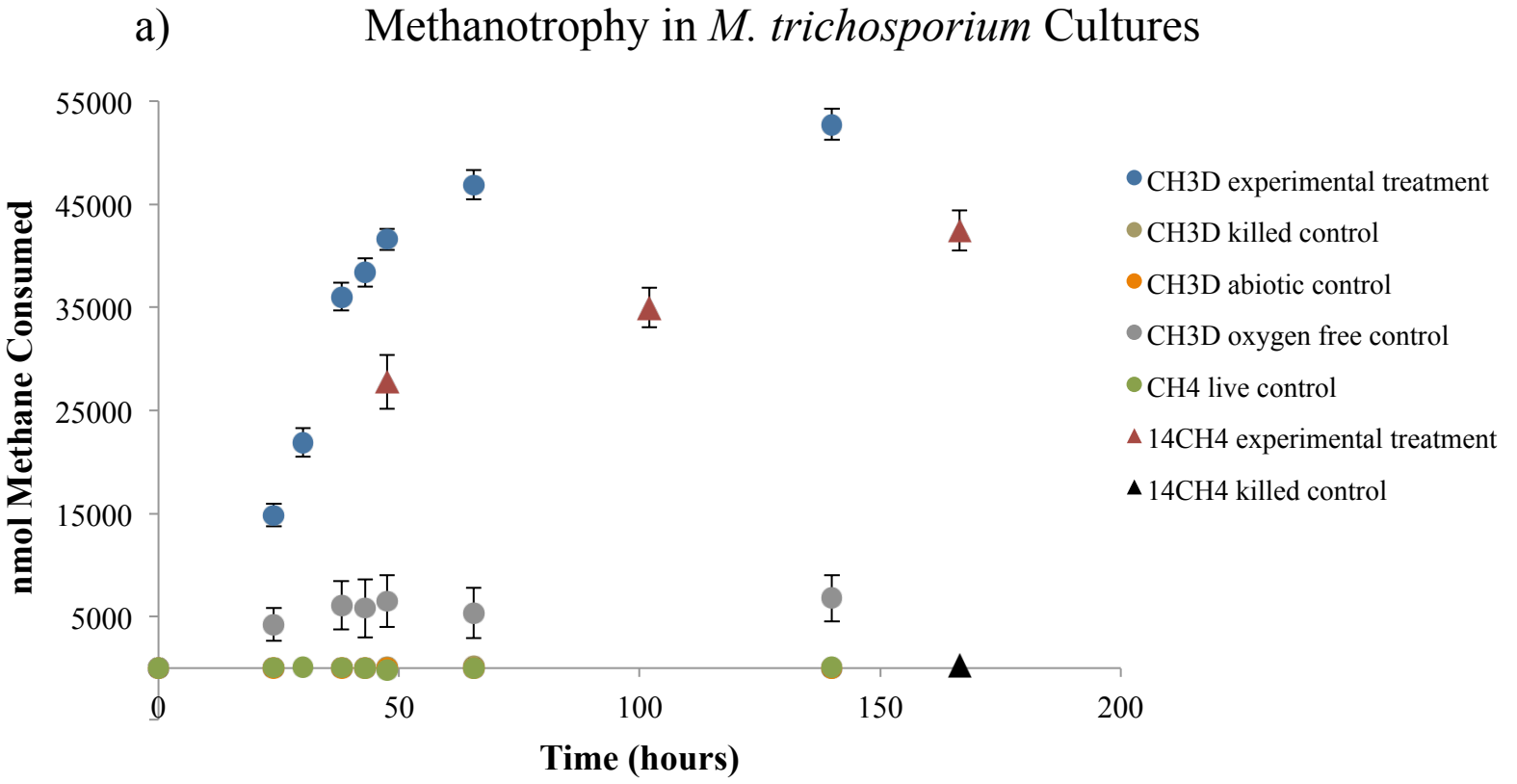
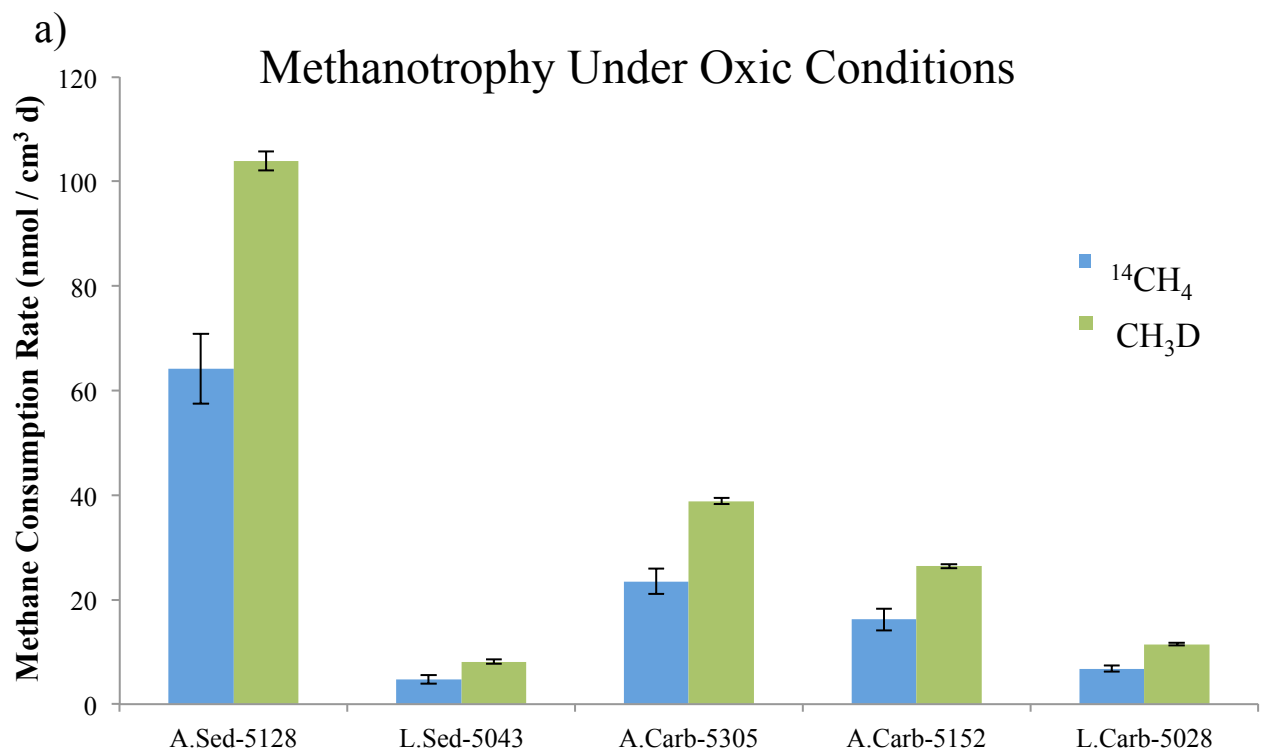


Figure 2



b)

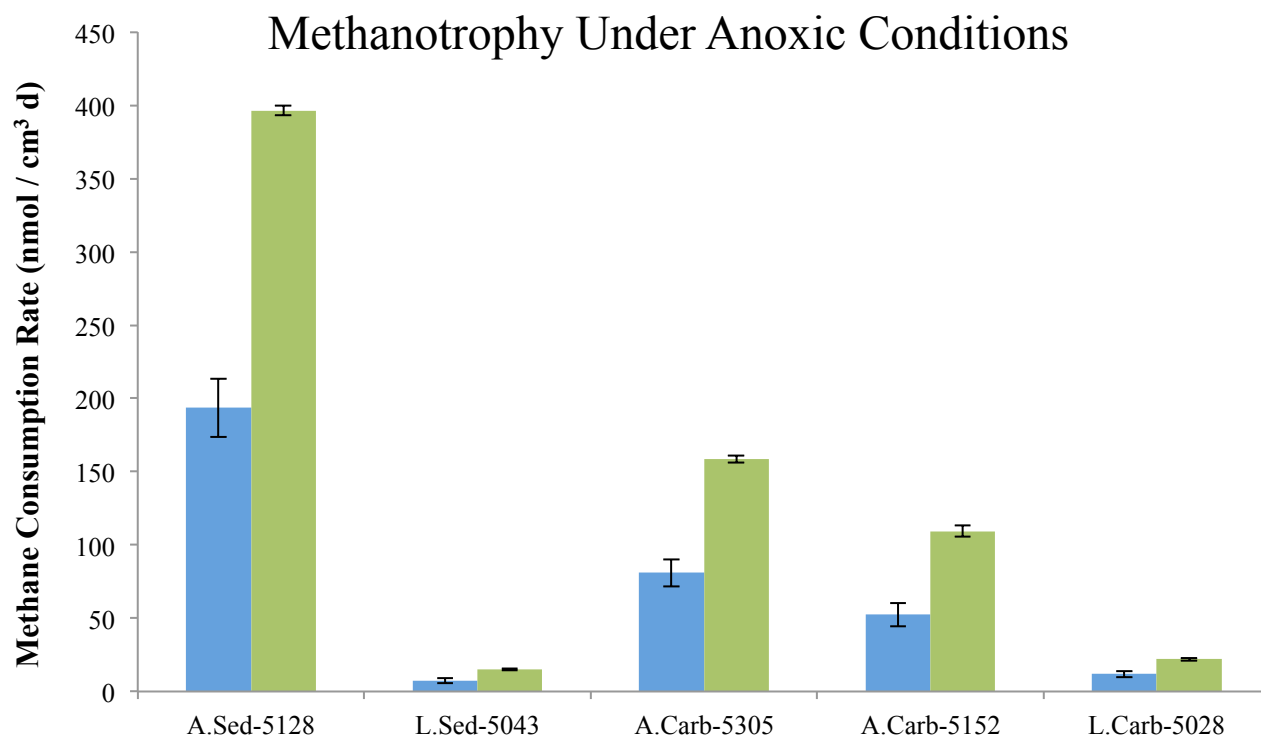


Figure 3

“Reverse Methanogenesis” Pathway

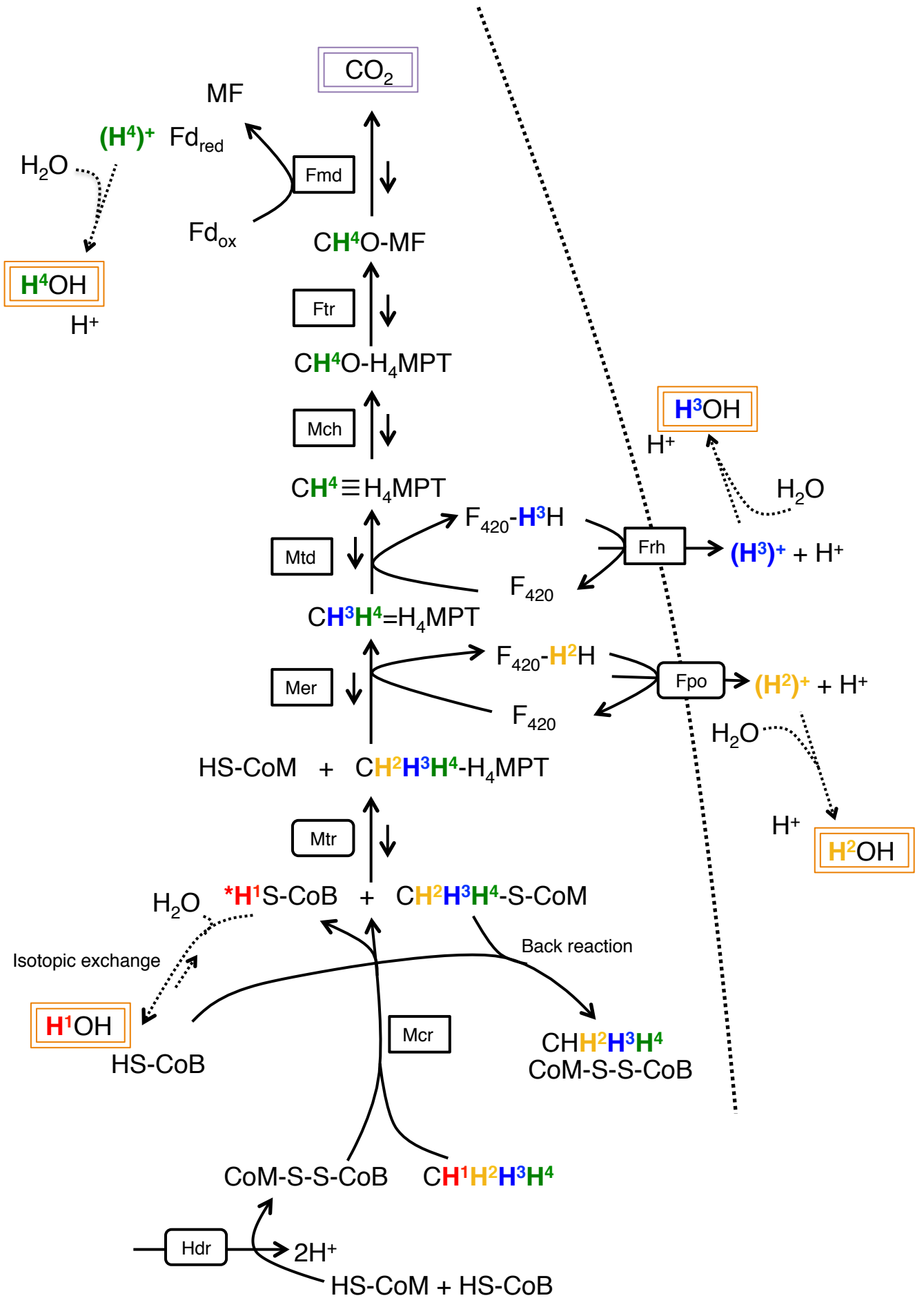


Figure 4

## Aerobic Methanotrophy Pathway

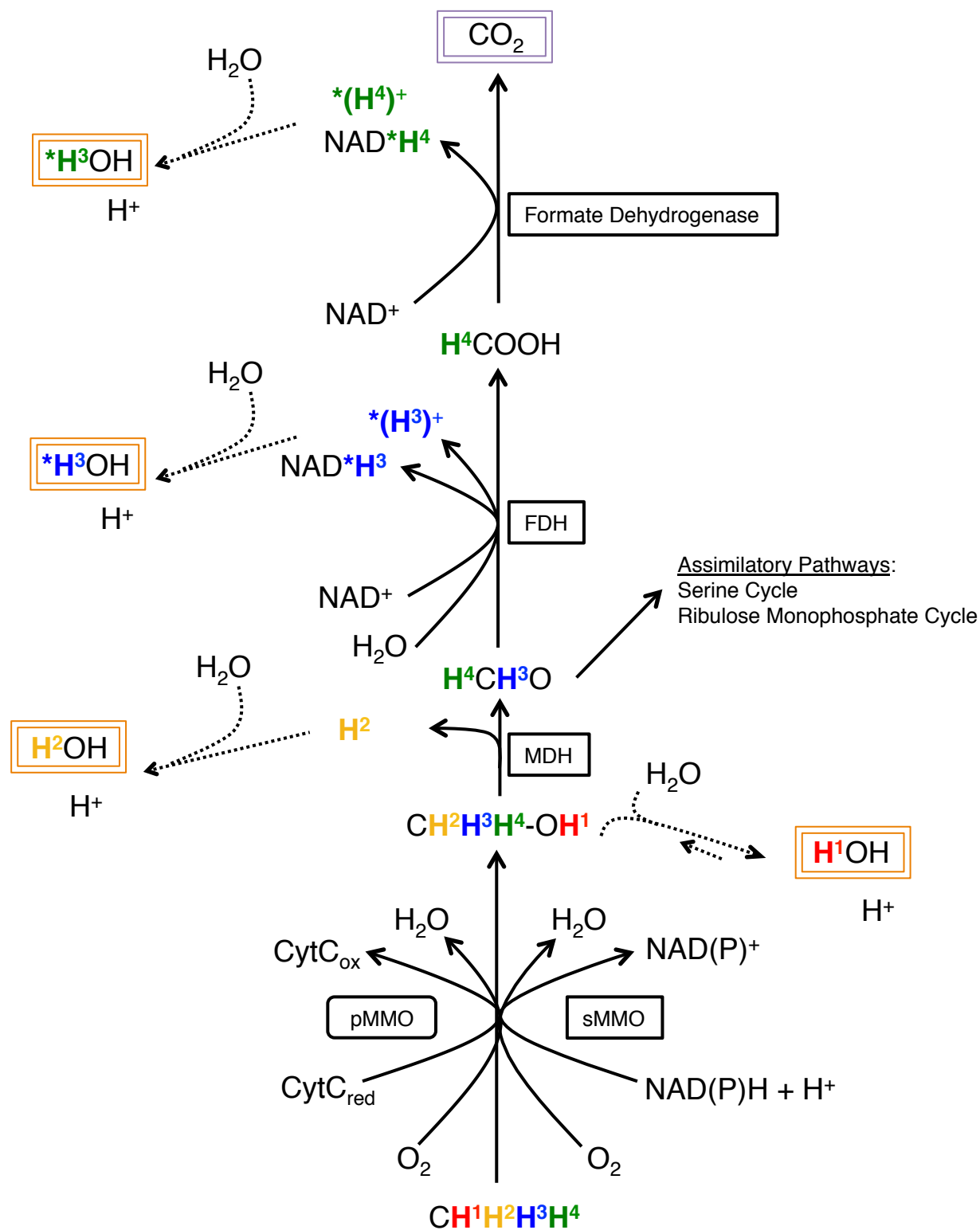


Figure 5

### Water $\delta D$ Values of Methane Seep Incubations at Atmospheric and Heightened Pressures

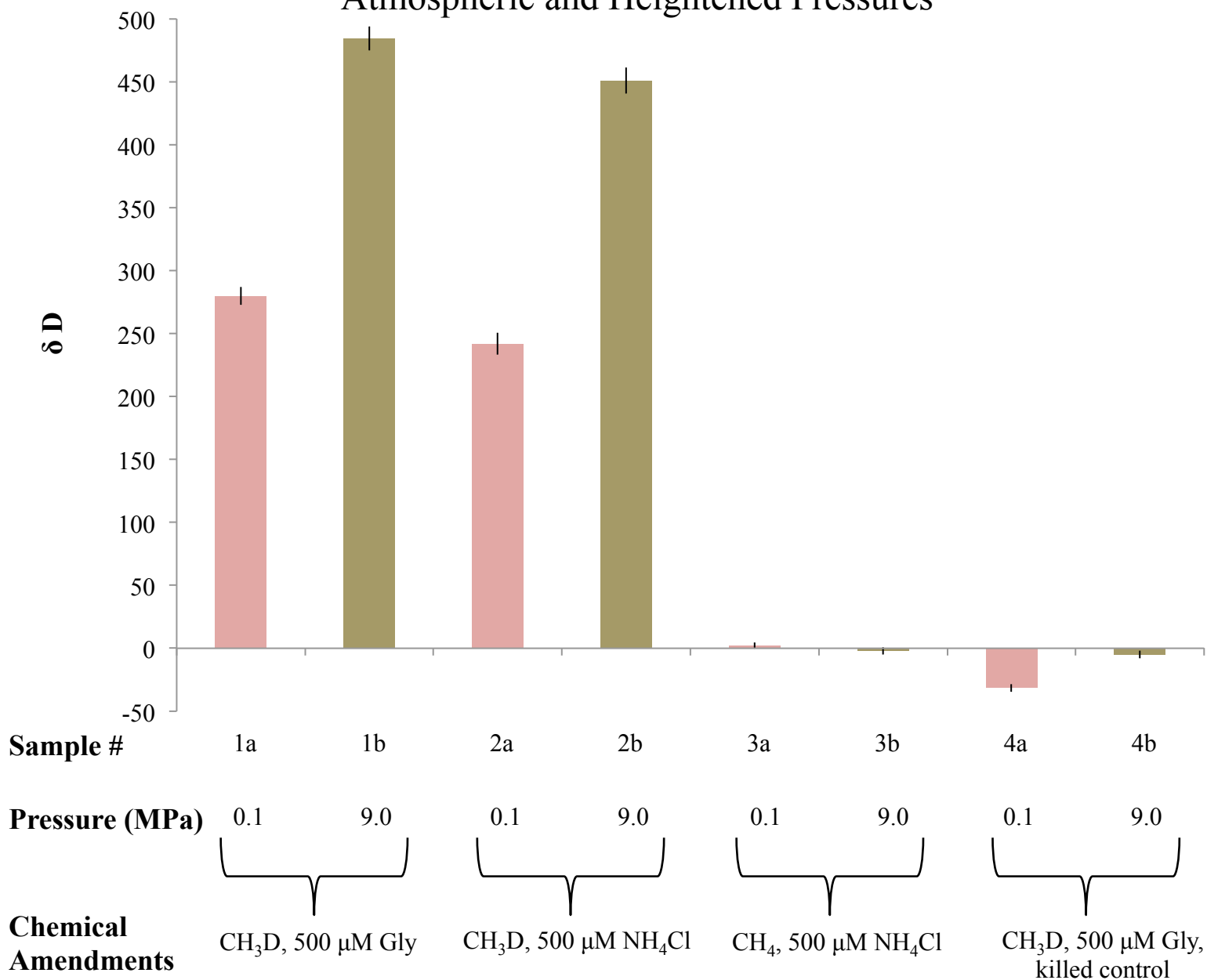
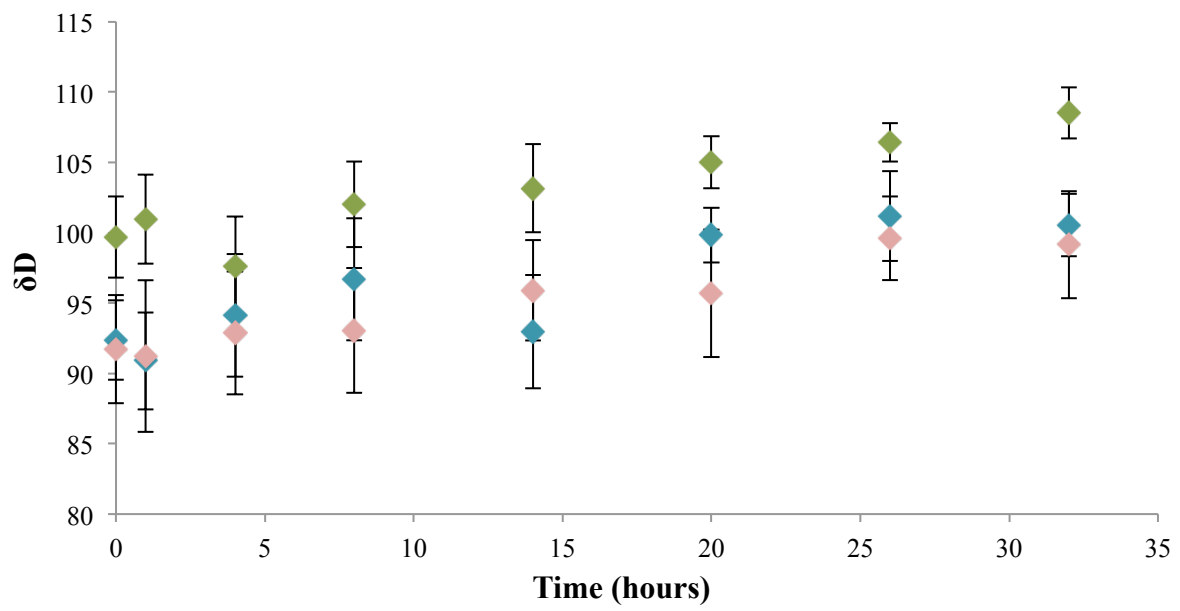




Figure S1



Supplementary Material for ““**Monodeuterated Methane: An Isotopic Probe to Measure Biological Methane Metabolism Rates and Track Catabolic Exchange Reactions**””

Table S1: Conditions for the aerobic methanotrophy experiments. All sample types were set up in triplicate; pressures shown as partial pressures.

Sample Condition	p(CH <sub>3</sub> D)	p(CH <sub>4</sub> )	<sup>14</sup> CH <sub>4</sub>	p(O <sub>2</sub> )	p(Ar)	Inoculum Introduced	Killed Cells
1	0.1 MPa			1 x 10 <sup>5</sup> Pa		10% v/v	
2	0.1 MPa			1 x 10 <sup>5</sup> Pa		10% v/v	Yes
3	0.1 MPa			1 x 10 <sup>5</sup> Pa			
4	0.1 MPa				1 x 10 <sup>5</sup> Pa	10% v/v	
5		0.1 MPa		1 x 10 <sup>5</sup> Pa		10% v/v	
6	0.1 MPa		13 kBq (T1)	1 x 10 <sup>5</sup> Pa		10% v/v	
7	0.1 MPa		13 kBq (T2)	1 x 10 <sup>5</sup> Pa		10% v/v	
8	0.1 MPa		13 kBq (T3)	1 x 10 <sup>5</sup> Pa		10% v/v	
9	0.1 MPa			1 x 10 <sup>5</sup> Pa		10% v/v	
10	0.1 MPa		13 kBq (T3)	1 x 10 <sup>5</sup> Pa		10% v/v	Yes

Table S2: The experimental set-up for methane seep sediment pressurized rate measurement incubations. The samples ran for 38 days at 4 °C, and each sample was contained in a sealed Mylar bag. Pressure values indicate absolute pressure exerted on the incubated Mylar bags.

Sample #	Sediment	Nitrogen Source	Methane Source	Pressure (MPa)
1a	50 mL	500 uM Glycine	40 mL CH <sub>3</sub> D	0.1
2a	50 mL	500 uM NH <sub>4</sub> Cl	40 mL CH <sub>3</sub> D	0.1
3a	50 mL	500 uM NH <sub>4</sub> Cl	40 mL CH <sub>4</sub>	0.1
4a	50 mL, killed control	500 uM Glycine	40 mL CH <sub>3</sub> D	0.1
1b	50 mL	500 uM Glycine	40 mL CH <sub>3</sub> D	9.0
2b	50 mL	500 uM NH <sub>4</sub> Cl	40 mL CH <sub>3</sub> D	9.0
3b	50 mL	500 uM NH <sub>4</sub> Cl	40 mL CH <sub>4</sub>	9.0
4b	50 mL, killed control	500 uM Glycine	40 mL CH <sub>3</sub> D	9.0

Fig. S1: To assess the empirical resolving power of the D/H measurement technique, we determined the time points showing non-overlapping confidence intervals for triplicate incubations of A.Sed-5128. Distinct signals were seen at the 20-hour time point for replicate A (teal diamonds) and the 26-hour time point for replicates B (pink diamonds) and C (green diamonds).

